energies

MDPI

*Article*

# An Intelligent Hybrid PIDF Enhanced by a Fuzzy Fractional-Order Controller for Robust Load Frequency Regulation in a Two-Area Interconnected Power System

**Saleh Almutairi [1,*], Fatih Anayi [1], Michael Packianather [1], Mohammad Almutairi [2] and Mokhtar Shouran [3]**

[1] School of Engineering, Cardiff University, Cardiff CF24 3AA, UK; anayi@cardiff.ac.uk (F.A.); packianatherms@cardiff.ac.uk (M.P.)
[2] College of Engineering and Energy, Abdullah Al Salem University, Kuwait City 12037, Kuwait; mohammad.almutairi@aasu.edu.kw
[3] Libyan Centre for Engineering Research and Information Technology, Bani Walid P.O. Box 38645, Libya; mokhta4520@gmail.com
* Correspondence: almutairis3@cardiff.ac.uk

## Abstract

Maintaining frequency regulation in interconnected power systems becomes increasingly difficult in the presence of nonlinear operating conditions. To address this issue, this study develops a hybrid load frequency control scheme in which a fuzzy fractional-order FOPI–FOPD controller is incorporated within a PIDF framework for a two-area LFC system. The controller parameters are optimized using the Dwarf Mongoose Optimization Algorithm (DMOA) and the Catch Fish Optimization Algorithm (CFOA), while the Integral of Time-Weighted Absolute Error (ITAE) is adopted as the performance criterion. The proposed strategy is examined under both linear and nonlinear scenarios, including the effects of Governor Dead Band (GDB) and Generation Rate Constraints (GRC). In the linear case, the DMOA-based design achieves an ITAE of 0.02939 with a tie-line settling time of 13.5478 s, whereas the CFOA-based design produces a bounded and convergent response with an ITAE of 0.03937 and a settling time of 14.4947 s. When GDB nonlinearity is introduced, the DMOA-tuned controller exhibits performance deterioration, yielding an ITAE of 0.1098 and a settling time of 19.0416 s, while the CFOA-tuned design shows more favorable time-domain performance with a lower ITAE of 0.05845 and a bounded settling time of 16.3595 s. These findings indicate that the CFOA-optimized PIDF–Fuzzy FOPI–FOPD controller provides an effective LFC solution under the examined nonlinear operating conditions.

**Keywords:** load frequency control; PIDF; fuzzy FOPI–FOPD; dwarf mongoose optimization; catch fish optimization



Academic Editor: Md. Abdus Salam

Received: 2 February 2026
Revised: 8 March 2026
Accepted: 10 March 2026
Published: 12 March 2026



## 1. Introduction

Load Frequency Control (LFC) plays a key role in preserving reliable operation of power systems during both planning and real-time operation. Variations in load demand, together with dynamic and stochastic disturbances, introduce uncertainties that can degrade frequency regulation [1]. Deviations from the nominal frequency may adversely affect grid dependability and power quality. In this context, LFC mitigates these effects by adjusting generator output dynamically, thereby reducing frequency deviations and keeping system variables within acceptable operating ranges. Accordingly, LFC remains an essential function in modern power-system operation [2].

A properly designed and well-managed power system should be capable of withstanding load fluctuations while delivering economical and high-quality electrical power. LFC contributes to this objective by improving dynamic performance, enforcing operating constraints, correcting generation-demand imbalance, and maintaining frequency deviations within permissible bounds. As a result, it supports reliable system operation, promotes economic dispatch, and helps satisfy prescribed performance requirements in power-system engineering [3].

### 1.1. Literature Review

Load Frequency Control (LFC) is fundamental to contemporary power system operations, crucial for sustaining stability and dependability against escalating system complexity and unpredictable load dynamics. The major purpose is to regulate generator output, mitigating frequency variations and tie-line imbalances resulting from load fluctuations. Decades of research have yielded a diverse array of solutions, from traditional linear controllers to sophisticated intelligence algorithms [4]. Nonetheless, a significant issue persists in identifying the most appropriate technique. No singular approach is universally superior; each involves trade-offs among robustness, flexibility, and complexity. Three principal factors restrict their efficacy: system nonlinearities, operational constraints, and regulatory stipulations [5,6]. The practical implementation of a successful LFC framework is exceedingly tough and necessitates considerable experience to navigate these intricate design trade-offs.

The proportional–integral–derivative (PID) controller remains a widely used element in LFC systems because of its simple structure, ease of implementation, and proven capability in controlling linear dynamic behavior. Its broad application in several engineering domains, including industrial automation, robotics, and process control, highlights its practical flexibility [7]. In LFC applications, frequency regulation is achieved by adjusting generator output through the proportional, integral, and derivative actions.

In Ref. [8], the Flood Algorithm (FLA) was applied to tune a PI controller in a two-area power system incorporating thermal and photovoltaic (PV) generation. The FLA-based controller achieved improved performance relative to earlier methods, including faster settling, smaller overshoot, and lower steady-state error under solar-irradiance and load-demand variations. Likewise, the Firefly Algorithm (FA) was applied in Ref. [9] to tune a PI controller for frequency regulation in a two-area PV-based system. In Ref. [10], Particle Swarm Optimization (PSO) was employed to identify the PID controller parameters of an isolated multi-source power system, resulting in enhanced frequency regulation and improved dynamic behavior under varying operating conditions. In Ref. [11], the Lyrebird Optimization Algorithm (LOA) was adopted to tune PID gains for a multi-source three-area power system, outperforming the controllers optimized by the African Vulture Optimization Algorithm (AVOA) and the Sand Cat Swarm Optimization (SCSO). In Ref. [12], the authors utilized the self-adaptive bonobo optimizer (SABO) to tune a PID controller for load frequency control in a two-area power system comprising a thermal plant and a wind farm. Likewise, Ref. [13] introduced a Rat Swarm Optimizer (RSO)-based PID controller that reduced settling time and frequency deviations while providing improved dynamic performance compared with traditional approaches under varying operating conditions.

Conventional PID controllers still face notable limitations when nonlinearities, parametric uncertainties, and communication delays arise in contemporary power systems. Such challenges have led to the development of advanced variants, such as fractional-order PID (FOPID), PID-Acceleration (PIDA), and Filtered/Double-Derivative PID (PIDF/PIDD) controllers. Further developments also include cascaded structures, such as PID–PI configurations, together with adaptive gain-scheduled schemes.

Utilizing fractional calculus, Fractional-Order Proportional–Integral–Derivative (FOPID) controllers employ non-integer-order integral and derivative actions, thereby expanding the controller design space and improving control flexibility. A considerable body of research has reported the effectiveness of FOPID controllers in modern power-system applications.

Reference [14] presented optimized PID and FOPID controllers for load frequency control (LFC) in a three-area thermal–wind–hydro system using several advanced meta-heuristic techniques, namely the Genetic Algorithm (GA), Grey Wolf Optimizer (GWO), Sine–Cosine Algorithm (SCA), and Atom Search Optimization (ASO), and assessed their performance under different cost functions. The reported results showed that the ASO-based FOPID controller achieved the most favorable transient behavior and robustness across varying operating conditions. In another study, Ref. [15] reported a FOPID controller for LFC in a two-area interconnected non-reheat thermal power system, with tuning performed using the Neural Network Algorithm (NNA), and examined under multiple load disturbance conditions. The proposed approach achieved superior ITAE minimization and dynamic response compared with conventional PID control and different optimization methods. In a similar vein, Ref. [16] considered a two-area multi-source deregulated power system employing an Aquila Optimizer (AO)-based FOPID controller for LFC applications. The proposed strategy delivered superior ITAE minimization and dynamic response across Poolco agreement, bilateral agreement, and varied operating conditions when compared with PSO- and WOA-based methods.

In addition to conventional PID-based structures, PID-Acceleration (PIDA) and Filtered/Double-Derivative PID (PIDF/PIDD) controllers have been introduced as advanced alternatives for addressing recent LFC demands. Reference [17] adopted hybrid tuning strategies that integrated Teaching–Learning-Based Optimization (TLBO), Tabu Search (TS), and the Equilibrium Optimizer (EDO) for Proportional-Integral-Derivative Adaptive (PIDA) controllers applied to a two-area configuration. This approach improved convergence rate, response quality, and tolerance to load disturbances and renewable intermittency. The reported simulation outcomes also showed that the TLBO–EDO-tuned PIDA controller surpassed conventional methods through reductions in oscillation amplitude, root mean square (RMS) values, and tie-line power deviations under multiple test conditions. In a related contribution, Ref. [18] employed a hybrid simulated annealing-based quadratic interpolation optimizer (hSA-QIO) to tune a proportional-integral-derivative with filter (PIDF) controller in a dual-area photovoltaic-thermal configuration. The hSA-QIO-tuned PIDF controller exhibited improved damping characteristics compared with traditionally tuned designs. Similarly, Reference [19] applied a Proportional–Integral–Double-Derivative (PIDD) controller within an IHPS, namely an isolated hybrid power system integrating conventional generation, renewable sources, energy storage, and electric vehicles (EVs). Its parameters were identified using the Magneto-Tactic Bacteria Optimization (MBO) method according to a peak-based integral square error (PISE) criterion. The reported findings indicated improved frequency regulation during simultaneous load and generation disturbances; however, several nonlinear effects, including generation rate constraints and governor dead bands, were omitted from the model.

These variants diminish susceptibility to high-frequency noise and enhance transient response, whereas PIDD architecture provides robustness under fluctuating loads. Nonetheless, PID-based controllers necessitate meticulous parameter adjustment and have restricted efficacy under strongly nonlinear or stochastic conditions. Such limitations have encouraged the emergence of more advanced control frameworks intended to surpass the intrinsic performance limits of linear designs. Sliding Mode Control (SMC): Owing to its capability in handling system uncertainty, SMC drives system trajectories toward a prescribed sliding surface. More recent developments in SMC-based LFC have led to

more advanced controller structures and improved tuning strategies. Reference [20] presented a decentralized full-order terminal sliding mode control (FOTSMC) scheme for load frequency control in multi-area power systems while considering communication delays as well as matched and unmatched disturbances. Its behavior was examined under load disturbances, inertia changes, and high renewable energy penetration. Comparison with conventional PI- and SMC-based methods showed that the proposed FOTSMC approach provided shorter settling time, lower peak overshoot and undershoot, and better performance under uncertain operating conditions.

Reference [21] introduced an improved super-twisting algorithm (ISTA) for sliding mode control in a multi-area power system integrating renewable energy sources and energy storage units. The ISTA-SMC method outperformed proportional-derivative and proportional-integral SMC schemes while effectively handling lumped disturbances associated with tie-line exchanges and renewable fluctuations. In addition, Reference [22] proposed a robust adaptive integral terminal sliding mode controller for load frequency control in interconnected power systems with renewable energy integration, with its parameters tuned using the Arithmetic Optimization Algorithm (AOA). The reported results showed lower overshoot, undershoot, and settling time, together with improved tolerance to parametric uncertainty, compared with the existing controller.

Although these studies demonstrated effective performance under different disturbance conditions, explicit representation of nonlinear dynamics was absent from these modeling approaches.

Linear Quadratic Regulator (LQR): The Linear Quadratic Regulator (LQR) has been employed in LFC mainly under linearized system assumptions. References [23,24] reported LQR-based designs without incorporating nonlinear effects into the system formulation. In [23], the use of a combined Cubature Kalman Filter and Linear Quadratic Regulator (CKF-LQR) scheme for load frequency control was investigated in both a single-area power system and a large-scale Egyptian power system with high renewable penetration. The reported results indicated that the proposed CKF-LQR approach achieved more accurate state estimation and superior frequency regulation performance than EKF-LQR, VSG-based control, and conventional PID-based schemes under measurement noise, low-inertia conditions, RES variations, and sudden load changes. Reference [24] applied an LQR design to a dual-area power network and evaluated its performance relative to conventional Proportional-Integral (PI) control under step-load disturbances, with emphasis on frequency control and dynamic response. Although both studies confirmed the value of optimal control in LFC applications, their dependence on linearized models reduces their applicability to practical systems with inherent nonlinearities.

Model Predictive Control (MPC): MPC-based approaches have shown considerable potential for LFC under different operating conditions. Reference [25] proposed a hybrid Grey Wolf Optimizer–Pattern Search (HGWO-PS)-tuned Model Predictive Control (MPC) scheme for an isolated dual-area microgrid. The proposed controller improved frequency regulation while reducing computational complexity.

Adaptive Control: Adaptive control strategies have also been explored to address LFC challenges in interconnected power systems. References [26,27] introduced adaptive frameworks intended to improve system response in the presence of disturbances and parametric variations. In Ref. [26], an adaptive PI controller was developed to adjust its gain online in response to changes in load demand and renewable energy inputs, including wind energy conversion systems (WECS) and PV-thermal systems. The reported controller exhibited better transient behavior and improved performance compared with traditional and optimized PID controllers. Reference [27] implemented a decentralized Model Reference Adaptive Control (MRAC) scheme for two-area systems using local

feedback signals together with a Lyapunov-based design framework. However, both adaptive approaches did not account for important nonlinear effects, such as governor dead bands and generation rate constraints, which may reduce their practical suitability in real power-system applications.

H-infinity Control (H∞): H∞ control provides a robust framework for handling system uncertainties and nonlinear effects in LFC applications. Reference [28] proposed a novel H∞/H2 pole-placement control scheme for load frequency control in interconnected power systems, where load disturbances were treated as measurable inputs to facilitate the synthesis of a low-order robust controller. The reported simulation results showed clear improvements over conventional PID and standard H∞/H2 controllers, including lower overshoot, much faster settling time, and a considerable reduction in control energy under load disturbances and parametric uncertainty. The proposed design also demonstrated scalability for extension to multi-area power networks.

Fuzzy Logic Control (FLC): FLC represents an effective alternative to conventional linear-feedback-based LFC in nonlinear, stochastic, and model-free environments. By relying on expert-defined linguistic rules, FLC supports decision-making under uncertain operating conditions. Its key advantages include the capability to manage nonlinearities [29], enhanced control performance [30], and seamless integration with hybrid control structures [31,32]. Nevertheless, the effectiveness of FLC remains strongly influenced by the configuration of the rule base and membership functions, which often demands meticulous tuning and may limit practical applicability.

Classical PID controllers are fundamental to LFC due to their structural simplicity and cost efficiency. Nonetheless, their constrained performance in the presence of nonlinearities and uncertainties has prompted the advancement of sophisticated methodologies:

- Advanced PID architectures, including FOPID and PIDA, provide superior robustness and adaptability relative to traditional designs, albeit with increased tuning complexity.
- Advanced control strategies (e.g., SMC, MPC, H∞) attain superior precision and disturbance rejection yet frequently entail increased computational and implementation requirements.
- Fuzzy Logic Control (FLC) offers an effective equilibrium of adaptability and feasibility, especially when incorporated into hybrid control systems, rendering it a compelling option for contemporary power systems.

Table 1 presents a comparative summary of representative LFC methodologies documented in prior research.

**Table 1.** Representative LFC approaches documented in prior research.

| Ref | Year | Control Scheme | Optimization Method | Renewable Sources | Nonlinear Effects | Nonlinearity Impact Analysis |
|---|---|---|---|---|---|---|
| [8] | 2025 | PI | FLA | ✓ | × | × |
| [9] | 2018 | PI | FA | ✓ | × | × |
| [10] | 2025 | PID | PSO | ✓ | × | × |
| [11] | 2024 | PID | LOA | ✓ | × | × |
| [12] | 2025 | PID | SABO | ✓ | × | × |
| [13] | 2024 | PID | RSO | × | × | × |
| [14] | 2023 | PID/FOPID | ASIA | ✓ | × | × |
| [15] | 2025 | FOPID | NNA | × | × | × |
| [16] | 2024 | FOPID | AO | × | × | × |
| [17] | 2025 | PIDA | TLBO | × | × | × |
| [19] | 2024 | PIDD | MBO | ✓ | × | × |

**Table 1.** *Cont.*

| Ref | Year | Control Scheme | Optimization Method | Renewable Sources | Nonlinear Effects | Nonlinearity Impact Analysis |
|---|---|---|---|---|---|---|
| [21] | 2025 | SMC | ISTA | ✓ | × | × |
| [22] | 2025 | SMC | AOA | ✓ | × | × |
| [23] | 2023 | LQR | - | × | × | × |
| [24] | 2024 | LQR | - | ✓ | × | × |
| [25] | 2023 | MPC | HGWO–PS | × | × | × |
| [26] | 2022 | Adaptive PI | - | ✓ | × | × |
| [27] | 2021 | MRAC | - | × | × | × |
| [28] | 2025 | H∞ | - | × | × | × |
| [29] | 2025 | Fuzzy PID | GWO | ✓ | ✓ | × |
| [30] | 2024 | Hybrid Fuzzy | QOAOA | × | × | × |
| [31] | 2023 | Hybrid Fuzzy | DE & GA | ✓ | ✓ | × |
| [32] | 2023 | Several hybrid Fuzzy structures | BA | × | × | × |

In this study, DMOA and CFOA were employed to tune the proposed hybrid PIDF + Fuzzy FOPI–FOPD controller, as both algorithms are well suited to nonlinear multi-parameter optimization tasks. DMOA has been utilized in engineering applications such as optimal power flow analysis in renewable-rich power systems [33] and solar PV parameter extraction [34]. Likewise, CFOA has been adopted in recent LFC studies for advanced controller tuning under nonlinear operating conditions [35,36].

### *1.2. Objectives and Contributions*

A notable limitation in current LFC research lies in the insufficient systematic assessment of nonlinear operating effects, particularly Generation Rate Constraints (GRC) and Governor Dead Band (GDB), on frequency control performance. Despite their acknowledged practical importance in realistic power-system operation, the impact of these nonlinearities has not been thoroughly examined, especially with respect to whether they are incorporated into or neglected from controller design and evaluation. As a result, the extent to which they influence closed-loop frequency behavior and overall system performance remains inadequately clarified. This shortcoming highlights the need for a more rigorous investigation into their operational consequences within LFC frameworks. To address this gap, the present study offers a systematic evaluation of the effects of GRC and GDB on frequency control performance.

#### 1.2.1. Challenges in LFC System Design

A key issue in LFC design is attaining an effective equilibrium between swift dynamic response and well-damped closed-loop behavior. Rapid transient correction is essential for prompt frequency recovery during load disturbances, reducing downtime and ensuring operational continuity. Excessively aggressive responses may result in overshoots that surpass safety thresholds, potentially jeopardizing delicate equipment. Conversely, slower corrective measures may improve damping and response smoothness but may allow temporary underfrequency or overfrequency fluctuations, thereby diminishing reliability during transitional phases. Consequently, optimal LFC strategies must balance the dual goals of swift stabilization and overshoot mitigation to guarantee both dynamic performance and secure operation.

#### 1.2.2. Limitations of Existing Control Strategies

LFC extensively uses Conventional PID controllers because of their structural simplicity, economic feasibility, and straightforward implementation. Nonetheless, their efficacy diminishes under nonlinearities, parametric uncertainty, and elevated system sensitivity—conditions that are increasingly common in contemporary power networks. PID controllers exhibit restricted efficacy in preserving frequency regulation performance amid dynamic load variations.

To address these shortcomings, several sophisticated control strategies have been investigated. Adaptive control adjusts gains online, enhancing tolerance to uncertainty; however, its computational burden and strict tuning demands limit broad practical adoption. Sliding Mode Control (SMC) provides inherent robustness against matched uncertainties, yet it is affected by chattering—high-frequency oscillations that may degrade performance and accelerate actuator wear. Fuzzy Logic Control (FLC) eliminates the requirement for explicit mathematical models by employing expert-defined linguistic rules. Nevertheless, numerous current FLC schemes still do not adequately handle performance variations under changing operating conditions, which reduces their dependability in evolving grid environments.

#### 1.2.3. Proposed Methodology and Contributions

The present study introduces an innovative hybrid PIDF + Fuzzy FOPI–FOPD controller for LFC. The proposed design adopts a parallel hybrid structure in which a PIDF branch operates alongside a cascaded fuzzy fractional-order compensation branch, thereby improving disturbance rejection, damping behavior, and robustness under nonlinear operating conditions.

The principal contributions of the present work are outlined as follows:

1. Proposed Hybrid Control Design: The proposed hybrid PIDF + Fuzzy FOPI–FOPD controller is designed using a parallel hybrid structure consisting of a PIDF branch and a cascaded fuzzy fractional-order compensation branch, whose parameters are subsequently optimized using DMOA and CFOA to achieve improved closed-loop time-domain performance, superior damping performance, and improved disturbance rejection.
2. Influence of Nonlinear Components: A systematic examination of generation rate constraints (GRC) and governor dead band (GDB) quantifies their impact on frequency regulation performance, offering essential insights into their function in contemporary LFC design.
3. Thorough Performance Assessment: Extensive comparisons with traditional controllers illustrate the superiority of the proposed scheme, achieving substantial reductions in overshoot, undershoot, and settling time while preserving robustness amid parametric uncertainties. Validation across various system configurations and operational conditions verifies its extensive applicability.
4. Robustness Validation: The DMOA and CFOA tuned controller reliably maintains bounded frequency responses during extreme stress conditions, such as sudden load fluctuations and $\pm 35\%$ parameter variations, underscoring its resilience and appropriateness for practical application.
5. Random Load Disturbance Validation: The proposed PIDF + Fuzzy FOPI–FOPD controller maintained bounded and convergent regulation responses with superior disturbance rejection under random load variations, achieving the lowest OS/US and the fastest ST compared with the benchmark controllers, which confirms its robustness under non-periodic load uncertainty.

This study enhances LFC controller design by incorporating fractional-order dynamics, fuzzy inference, DMOA and CFOA-based optimization, providing an adaptive, robust, and scalable solution for contemporary power systems, surpassing traditional and advanced methodologies.

### *1.3. Paper Structure*

The remainder of this paper is organized as follows. Section 2 presents the mathematical framework of the studied power system, including parameter specifications and the explicit modeling of GRC and GDB. Section 3 describes the proposed LFC architecture, the optimization procedure, and the formulation of the cost function used for controller design. Section 4 reports the simulation-based validation, including comparative performance analysis under different operating scenarios and the robustness evaluation of the DMOA- and CFOA-tuned FLC under parametric uncertainty and random load disturbances. Finally, Section 5 concludes the paper by summarizing the main findings, outlining the theoretical and practical implications, and suggesting directions for future research.

## 2. Power Systems Under Study: Modeling and Parameters

The present study performs a comparative assessment of two power-system models to evaluate the behavior of the proposed fuzzy control framework. The first model incorporates governor dead band (GDB) nonlinearities to assess their influence on frequency regulation behavior, whereas the second model includes generation rate constraint (GRC) dynamics to examine their effect on system response. Taken together, these case analyses confirm the effectiveness of the proposed configuration in handling nonlinear characteristics encountered in modern power-system operation.

### *2.1. First Power System Model*

The present subsection considers a reference dual-area interconnected power-system model that is widely used in LFC studies. The configuration consists of two asymmetrically parameterized areas connected through a tie-line and includes the usual elements, including governors, turbines, load dynamics, and synchronous generating units, to represent realistic operating conditions. The schematic representation appears in Figure 1, while the corresponding parameter values are provided in Appendix A [37].

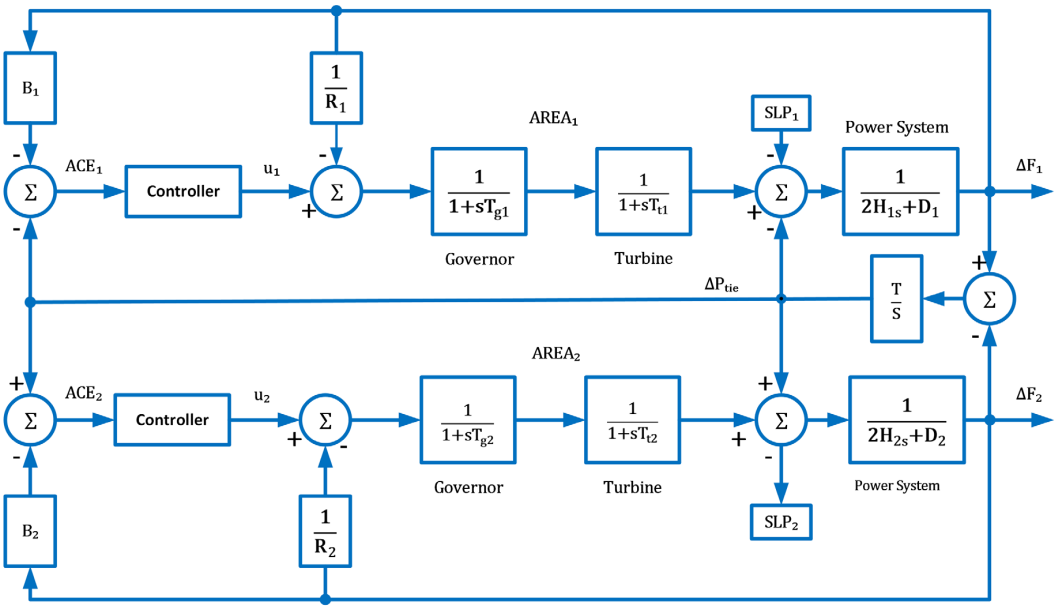


**Figure 1.** Schematic representation of the first analyzed power system model [36].

LFC design is based on the Area Control Error (ACE), which serves as a key feedback signal by combining frequency deviation and tie-line power mismatch to generate corrective control action. In this framework, the ACE expressions for Areas 1 and 2 are given in Equations (1) and (2), forming the basis for frequency regulation under dynamic load disturbances.

$$ACE_1 = \Delta P_{12} + B_1 \Delta F_1 \quad (1)$$

$$ACE_2 = \Delta P_{21} + B_2 \Delta F_2 \quad (2)$$

The variables $\Delta F_1$ and $\Delta F_2$ represent the frequency deviations in Areas 1 and 2, respectively. Similarly, $\Delta P_{12}$ and $\Delta P_{21}$ denote the tie-line power-flow deviations, while $B_1$ and $B_2$ indicate the frequency bias coefficients associated with each area.

### *2.2. Governor Dead Band (GDB) Modeling and Integration*

The Governor Dead Band (GDB) is a physical nonlinearity associated with turbine-governor systems and can be defined as a threshold region within which small frequency deviations do not produce corrective valve action. This effect mainly arises from two sources: (i) mechanical tolerances in valve positioning that create slack, and (ii) intentional signal filtering introduced to reduce unnecessary actuator movement during transient events. As a result, the governor response is delayed, which introduces phase lag, increases power oscillations, and reduces the effectiveness of LFC.

For a more realistic representation of turbine-governor dynamics, GDB nonlinearity is embedded in the overall plant model following the analytical description reported in Reference [38]. This representation characterizes the valve dead zone that appears under small speed deviations. Accordingly, the resulting governor transfer function with GDB included is given by:

$$G_{GDB}(s) = \frac{-\frac{0.2}{\pi}s + 0.8}{T_g s + 1} \quad (3)$$

Tg is the governor time constant. The numerator contains the terms 0.8 and $-\pi$, which capture the unequal dead-band effect on valve motion, as stated in Ref. [38]. This nonlinear block is embedded within the governor path of the system illustrated in Figure 1 to evaluate the closed-loop response under practical non-ideal conditions and to study its behavior under realistic dynamic variations.

### *2.3. Second Power System Model*

To extend the evaluation of the proposed control strategy, the controller is applied to an additional benchmark platform, thereby improving the credibility and practical relevance of the study. Figure 2 shows an interconnected two-area configuration equipped with a non-reheat thermal generating unit. The principal parameters, including nominal frequency (Fi, Hz), regulation coefficient (Ri, Hz/unit), governor time constant (Tgi, s), turbine time constant (Tti, s), and the time constant of the power system (Tpi, s), are specified to represent the dynamic behavior of the plant.

The model incorporates key state variables, namely area control error (ACEi), load-demand variation (ΔPDi), speed changer adjustment (ΔPci), governor valve displacement (ΔPgi), power gain coefficient (KPi), and tie-line power variation (ΔPtie). The complete set of parameter values is provided in Appendix B [39].

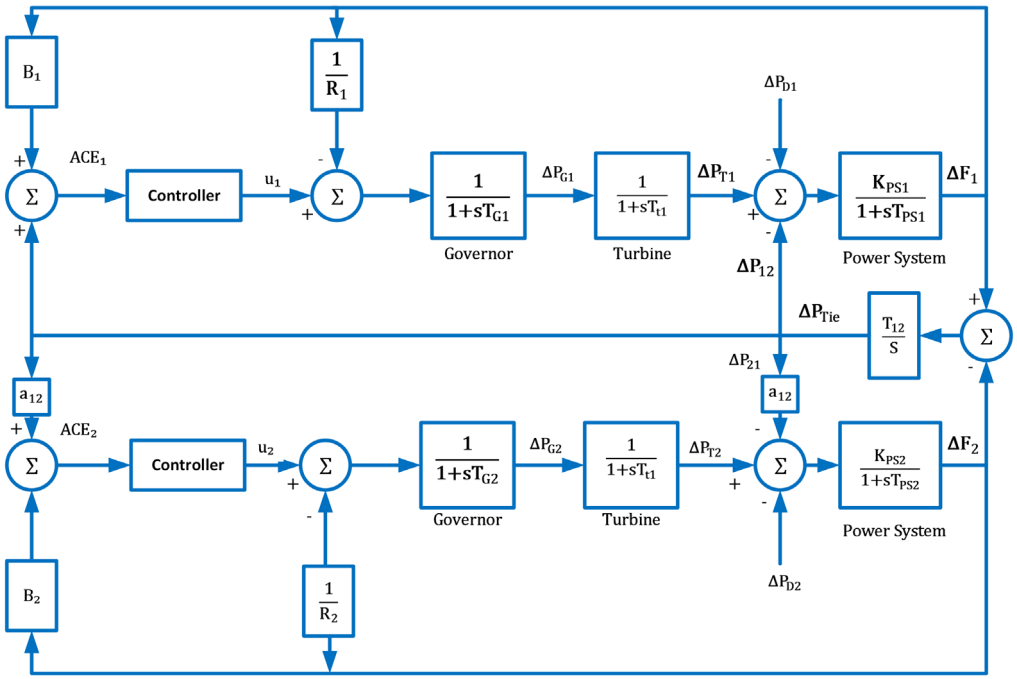


**Figure 2.** Schematic representation of the second analyzed power system model [36].

### *2.4. Generating Rate Constraints (GRC) Representation and Implementation*

GRC defines the allowable rate at which a generating unit may raise or lower its output, under the influence of turbine thermal behaviour, mechanical inertia, and secure operating requirements. It is generally formulated as bidirectional ramp-rate limits on turbine output to preserve safe and feasible operation. When GRC is omitted from dynamic studies, the computed response can appear excessively rapid and may fail to represent actual plant behaviour.

To account for this effect, the conventional non-reheat turbine representation in Figure 2 is replaced with the nonlinear arrangement illustrated in Figure 3, where the rate limit is fixed at $\alpha = \pm 0.025$ pu/s. A saturation function is employed to bound changes in turbine output, thereby reproducing the slower behaviour introduced by inertial and heat-transfer effects. As indicated in Ref. [39], this representation keeps the turbine response within feasible operating ranges and prevents unrealistically optimistic simulation results.

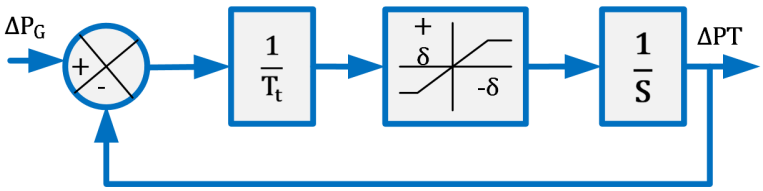


**Figure 3.** Nonlinear turbine model using GRC [36].

Reference [40] states that the inclusion of GRCs is necessary for a realistic assessment of LFC schemes, since excluding them may yield excessively favorable predictions of control responsiveness and overall transient behavior. Incorporating GRCs within the turbine model therefore offers a more representative basis for evaluating system frequency control and inter-area tie-line power transfer under variable operating scenarios.

## 3. The Proposed Controller and Tuning Tool

### *3.1. The PIDF Plus Fuzzy FOPI–FOPD Architecture*

This study improves the foundational PIDF controller by embedding an intelligent fuzzy-based control mechanism within its structure to achieve an effective LFC configuration, as illustrated in Figure 4. Fuzzy Logic Control (FLC), known for its robustness under varying operating conditions, is employed to enhance the adaptability and regulation quality of the overall control action. By integrating fuzzy reasoning with the PIDF dynamics, the proposed control scheme provides improved frequency regulation performance while maintaining a coherent and unified control architecture.

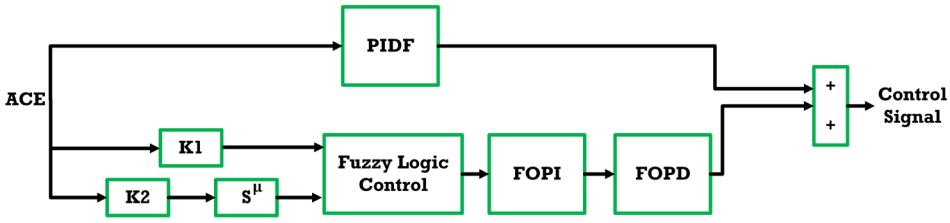


**Figure 4.** Parallel hybrid PIDF + fuzzy FOPI–FOPD control structure.

The DMOA and CFOA are employed to tune the parameters of the proposed hybrid controller with the objective of enhancing overall LFC performance. As shown in Figure 4, the proposed controller adopts a parallel hybrid structure composed of two branches. The first branch is a PIDF controller acting directly on the ACE signal, whose transfer function is given in Equation (4). The second branch is a fuzzy fractional-order compensation path, in which the ACE signal and its derivative are processed by the fuzzy logic unit and then passed through cascaded FOPI and FOPD blocks. The transfer functions of the FOPI and FOPD blocks are presented in Equations (5) and (6), respectively. The outputs of the two branches are finally summed to generate the overall control signal.

$$\mathrm{PIDF_c(S)} = \mathrm{K_p} + \frac{\mathrm{K_i}}{\mathrm{S}} + \frac{\mathrm{K_d K_F}}{1 + \mathrm{K_F}\frac{1}{\mathrm{S}}} \tag{4}$$

$$C_{\mathrm{FOPI}}(s) = K_{p1} + \frac{K_{i1}}{s^{\lambda}} \tag{5}$$

$$C_{\mathrm{FOPD}}(s) = K_{p2} + K_{d2}s^{\mu} \tag{6}$$

The fuzzy logic unit receives the scaled ACE signal and its derivative through the $K_1$ and $K_2$ channels, respectively, and generates an intermediate nonlinear compensating signal. This signal is subsequently processed by the cascaded FOPI and FOPD blocks, while $K_3$ acts as the output scaling factor of the fuzzy compensation path before final summation with the PIDF branch.

Due to the nonlinear, rule-based nature of the fuzzy inference layer, the proposed controller is more appropriately described as a composite hybrid control law rather than a single global linear transfer function.

This hybrid design integrates the adaptive reasoning capability of fuzzy logic with the deterministic characteristics of the PIDF framework to enhance overall control performance within a unified control structure. The Fuzzy Logic Controller (FLC) is implemented with an emphasis on structural simplicity and computational efficiency. It employs five trapezoidal and triangular membership functions for each linguistic input and output variable, as illustrated in Figure 5: Negative Big (NB), Negative Small (NS), Zero (Z), Positive Small (PS), and Positive Big (PB). The control action is governed by a fuzzy rule base consisting of 25 conditional rules, as summarized in Table 2.

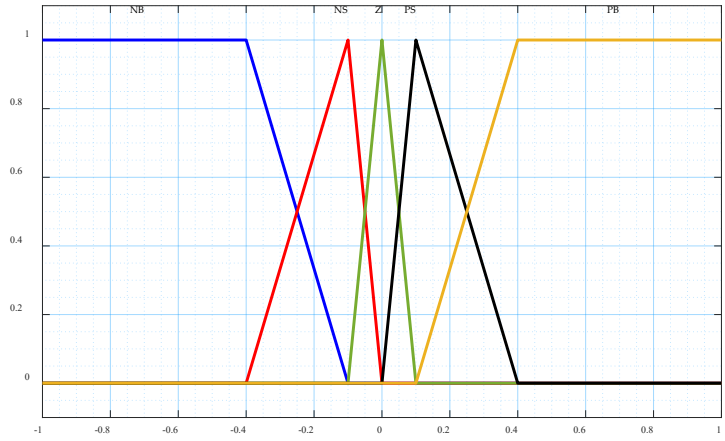


**Figure 5.** Fuzzy Controller Membership Functions [36].

**Table 2.** FLC Component Rule Set [36].

| Error | Change in Error | | | | |
|---|---|---|---|---|---|
| | **NB** | **NS** | **Z** | **PS** | **PB** |
| NB | NB | NB | NB | NS | Z |
| NS | NB | NB | NS | Z | PS |
| Z | NB | NS | Z | PS | PB |
| PS | NS | Z | PS | PB | PB |
| PB | Z | PS | PB | PB | PB |

These membership functions were arranged with suitable overlap to provide smooth transition between adjacent linguistic regions. The 25-rule base was formulated according to the conventional LFC logic based on the ACE signal and its rate of change, such that large deviations yield strong corrective action, whereas small deviations near the operating point result in mild compensation. In addition, Mamdani inference with centroid defuzzification was adopted to generate a smooth crisp output for the fractional-order compensation path.

The gain parameters of the integrated PIDF + Fuzzy FOPI–FOPD controller, including ($K_1$, $K_2$, $K_3$, Kp, Ki, Kd, λ, μ), are tuned by the DMOA and CFOA within a unified optimization framework. The crisp input signals are fuzzified using the Mamdani inference mechanism to generate fuzzy linguistic variables. Subsequently, de-fuzzification is performed via the centroid method, which determines the center point of the combined output distribution and produces the final real-valued control signal.

The fractional orders $\lambda$ and $\mu$ constitute key elements in defining the dynamic characteristics of the proposed control scheme. The fractional integral order $\lambda$ is associated with memory properties that support long-memory behavior and steady-state regulation, whereas the fractional derivative order $\mu$ provides additional flexibility in shaping transient behavior and enhancing damping performance. The inclusion of these fractional orders extends the tuning freedom of the controller, allowing its dynamic response to be adjusted more effectively to meet the overall frequency regulation objectives.

For reproducible implementation of the fractional-order controller, the FOPI and FOPD terms were realized in MATLAB/Simulink (2024a) using the FOMCON toolbox based on the Oustaloup recursive approximation. In particular, the fractional operators were approximated in continuous time over the frequency range [ωb, ωh] = [0.001, 1000] rad/s with an approximation order of N = 5. These settings were maintained unchanged throughout all simulations and for both optimization algorithms to ensure a consistent and verifiable implementation framework.

### *3.2. The Suggested Tuning Tool: Catch Fish Optimization Algorithm*

The Catch Fish Optimization Algorithm is a population-based metaheuristic inspired by conventional fishing activities, in which fishermen are represented as autonomous search entities. The method operates through two principal modes: an exploration mode, where agents examine promising regions independently, and an exploitation mode, where cooperative actions are used to surround and refine candidate solutions near the current optimum. The shift between these two modes is adaptively governed by a stochastic capture-rate coefficient ($\alpha$), enabling a suitable trade-off between diversification and intensification. Previous studies [36] have shown that CFOA is appropriate for controller tuning in systems containing nonlinear components such as GRC and GDB because it preserves a suitable trade-off between global and local search. This characteristic supports its adoption in the present work, where such nonlinear effects are significant. To reduce computational burden during optimization, the population size and maximum number of iterations were set to 50 and 100, respectively. Additional details on CFOA, including its operating mechanism, flowchart, and mathematical expressions, are available in Refs. [36,41].

(1) Exploration Phase

At this stage, the method reproduces the initial fishing process in which fishermen search individually for fish-rich regions. Each agent performs a localized search and introduces hydrodynamic disturbance effects to strengthen detection capability. As resource distribution changes, the search progressively moves from isolated activity to cooperative group movement.

- ➢ Individual Search: Each agent explores the search domain independently to identify concealed opportunities.
- ➢ Capture-Rate Evaluation ($\alpha$): A probabilistic rule determines whether the agent remains in individual search mode or shifts to collaborative movement.
- ➢ Position Adjustment: Agent locations are updated according to local success and observed tendencies, either refining the current trajectory or relocating to alternative regions when required.

(2) Exploitation Phase

At this stage, the fishermen act cooperatively to concentrate the search around the most promising regions identified earlier. Agents interact spatially and use herding and surrounding actions to increase capture effectiveness.

- ➢ Cluster Formation: Agents gather in small teams, usually composed of 3–4 members, around selected target areas and establish a centroid-based reference point.
- ➢ Cooperative Surrounding: These teams follow Gaussian-based spatial arrangements, with central agents concentrating on the principal targets while outer agents restrict potential escape routes.
- ➢ Global-Best Guidance: Position updates are referenced to the best solution found so far, while step magnitudes are adaptively adjusted to enhance precision.

Together, these mechanisms allow CFOA to preserve a useful balance between broad search and local refinement, thereby improving convergence rate and solution quality.

### *3.3. The Suggested Tuning Tool: DMOA*

The Dwarf Mongoose Optimization Algorithm (DMOA) is a metaheuristic optimization method inspired by the social organization and collaborative behavior of dwarf mongooses. It models the population as independent search agents grouped into the alpha group, scouts, and babysitters, and operates through two main phases: exploration, where the alpha group and scouts seek new regions and viable solutions, and exploitation, where

the population converges to refine high-quality areas in the search space. DMOA adaptively shifts between these modes via the babysitter-exchange mechanism and a dynamic collective-movement coefficient, maintaining a balance between diversification and intensification. Recent studies [42] report that DMOA achieves high-quality solutions and can outperform several commonly used optimizers, supporting its suitability for this task. To limit computational overhead, the population size and iteration count were set to 50 and 100, respectively. Further details, including the flowchart and mathematical formulation, are provided in Ref. [42].

(1) Exploration Phase

During this phase, the algorithm emulates the initial dispersal behavior of dwarf mongooses as they seek new foraging areas. The alpha group and scouts function as autonomous search agents, executing semi-nomadic movements to expand the exploration radius and prevent premature convergence.

- ➢ Independent Scouting: Alpha members and scouts engage in solitary investigative actions across various "mounds," examining distinct regions of the search space to identify potential areas of interest.
- ➢ Evaluate Mound Quality: Each examined location is evaluated using a mound-quality metric that indicates the relative performance of the current area. Inferior mounds necessitate relocation, promoting ongoing diversification.
- ➢ Dynamic Position Updating: Agents modify their trajectories in response to local success and environmental cues, either enhancing their current positions or relocating to new mounds when exploration ceases to yield results.

(2) Exploitation Phase

In this phase, the population transitions from widespread exploration to focused refinement in the most promising areas previously identified. The groups collaborate to systematically enhance local searches.

- ➢ Babysitter-Exchange Mechanism: A systematic exchange transpires between foraging groups and the babysitter cohort, enabling rested individuals to participate in exploitation activities and sustaining swarm vitality while regulating exploration pressure.
- ➢ Cooperative Local Search: Agents work together to narrow their search area and focus on high-quality mounds. This makes the search more accurate and helps agents converge on the best areas.
- ➢ Alpha-Best Referencing: Position updates are directed by the optimal solution identified by the alpha group, with displacement magnitudes diminishing over time—facilitating refinement in proximity to optimal regions while maintaining slight stochasticity to avert stagnation.

Collective Dynamics

Collectively, these mechanisms allow DMOA to sustain a robust equilibrium between exploratory diversification and exploitative refinement, markedly affecting convergence speed, solution quality, and overall convergence reliability.

### *3.4. Cost Function*

In control engineering, achieving a proper balance between fast transient response and sufficiently damped closed-loop performance remains a central design issue. These requirements are often conflicting, because accelerating the transient response may weaken damping characteristics and response smoothness, whereas excessive damping can slow the overall system dynamics. Accordingly, a sound control strategy should handle this

balance through proper controller configuration and the optimization of a suitable objective function, often by employing modern optimization algorithms.

Several error-based criteria are frequently used to assess control-system performance, including the Integral of Time-Weighted Absolute Error (ITAE), Integral of Squared Error (ISE), Integral of Time-Weighted Squared Error (ITSE), and Integral of Absolute Error (IAE). Among these measures, ISE and ITAE are the most adopted in previous studies, since they often deliver more desirable dynamic characteristics than IAE- or ITSE-based formulations.

Under the ISE criterion, the squared error is accumulated over time, which imposes a quadratic penalty on large deviations. Consequently, high-amplitude errors are strongly reduced, although small residual deviations may persist. Therefore, controllers designed with ISE often show a rapid initial response but may retain low-amplitude oscillations over a longer portion of the settling interval. By comparison, the ITAE criterion evaluates the absolute error with time weighting, thereby assigning greater significance to errors that remain for longer periods. Because of this temporal emphasis, ITAE-based tuning commonly produces shorter settling times and improved transient characteristics relative to ISE-based designs.

In this study, the LFC controller gains are tuned using the Dwarf Mongoose Optimization Algorithm (DMOA) and the Catch Fish Optimization Algorithm (CFOA). For both methods, the selected objective is the minimization of the Integral of Time-Weighted Absolute Error (ITAE), which can be written mathematically as:

$$\text{Cost function} = ITAE = \int_0^t |e| \cdot t.dt \tag{7}$$

## 4. Results and Discussion

### *4.1. Scenario 1: Power System 1 Without Nonlinearities*

This subsection examines the time-domain response of the two-area power system illustrated in Figure 1 when a 0.2 pu step load perturbation is introduced in Area 1. The proposed fuzzy-based LFC scheme is tuned through the DMOA and CFOA to compare their impact on system performance. Each optimizer was run for 100 iterations, where the fuzzy-controller parameters were searched within [0, 2], while the PIDF derivative filter coefficient $K_f$ was adjusted over the wider range [0, 500].

The simulation results offer a comprehensive assessment of the effectiveness of the DMOA and CFOA in tuning the proposed PIDF + Fuzzy FOPI–FOPD controller for the investigated power system. The statistical evaluation is conducted over 10 independent runs, where the minimized ITAE values achieved by DMOA and CFOA are compared. Figure 6 visually presents the minimized ITAE values according to the run number. In parallel, Table 3 reports the detailed statistical outcomes, including the best, mean, median, worst, and standard deviation values for both optimization methods.

All 10 runs were conducted under identical tuning conditions, using the same ITAE cost function, parameter bounds, population size, and iteration budget for both DMOA and CFOA. The results demonstrate that DMOA surpasses CFOA across all evaluated statistical measures. DMOA attains a lower best ITAE value (0.02939) than CFOA (0.03937). Likewise, the mean, median, and worst ITAE values remain consistently smaller for DMOA, confirming its stronger capability in reducing the ITAE criterion. Moreover, the standard deviation associated with DMOA (0.000351) is lower than that obtained with CFOA (0.000391), which reflects a more consistent and dependable optimization performance.

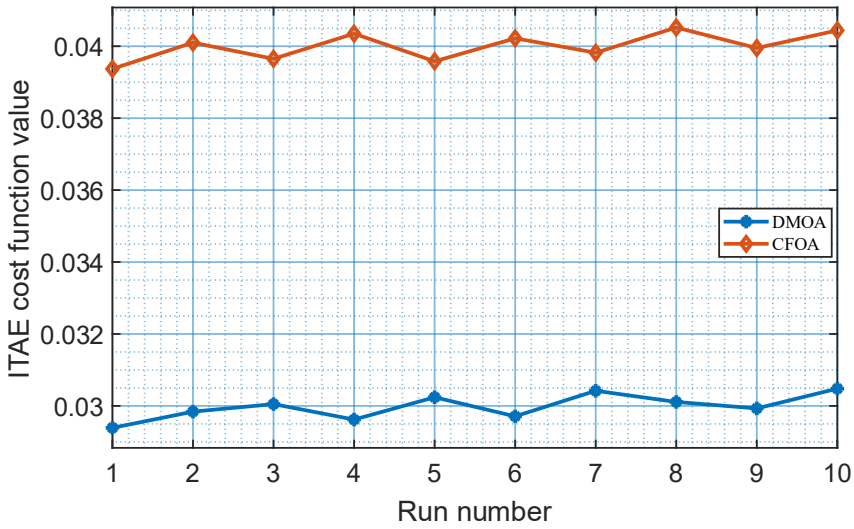


**Figure 6.** Minimized ITAE values from 10 independent runs of DMOA and CFOA.

**Table 3.** Statistical results obtained for DMOA and CFOA.

| Metric | DMOA | CFOA |
|---|---|---|
| Best | 0.02939 | 0.03937 |
| Mean | 0.029979 | 0.040000 |
| Median | 0.029990 | 0.040025 |
| Worst | 0.03048 | 0.04052 |
| Standard deviation | 0.000351 | 0.000391 |

The PIDF + Fuzzy FOPI–FOPD controller was tuned using the DMOA and CFOA. The convergence profiles of both optimization procedures are shown in Figure 7, where the variation in the cost function throughout the search process can be observed. Moreover, the final controller parameter values obtained from each algorithm are reported in Table 4 and are then used to assess the dynamic performance of the system.

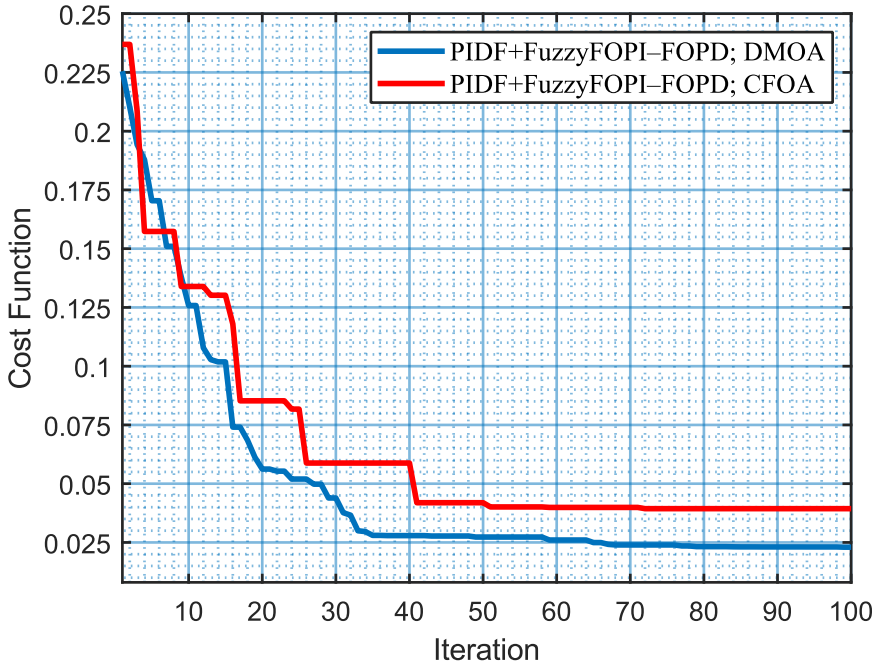


**Figure 7.** The convergence curves of DMOA and CFOA.

**Table 4.** Optimized Parameter Values of the PIDF + Fuzzy FOPI–FOPD Controller.

| **Area** | **Controller** | **Algorithm** | **Parameters** | | | | | | | | |
|---|---|---|---|---|---|---|---|---|---|---|---|
| Area One | PIDF | | $K_p$ | | $K_i$ | | $K_d$ | | | $K_f$ | |
| | | DMOA | 0.57987 | | 1.9393 | | 0.55162 | | | 451.09 | |
| | | CFOA | 1.367 | | 1.9951 | | 0.86544 | | | 355.42 | |
| Area Two | | | $K_p$ | | $K_i$ | | $K_d$ | | | $K_f$ | |
| | | DMOA | 1.1385 | | 1.809 | | 1.7901 | | | 185.7 | |
| | | CFOA | 1.8508 | | 1.3512 | | 1.5548 | | | 83.08 | |
| **Area** | **Controller** | **Algorithm** | **Parameters** | | | | | | | | |
| Area One | Fuzzy FOPI–FOPD | | $K_1$ | $K_2$ | $K_3$ | $K_{p1}$ | $K_{i1}$ | λ | $K_{p2}$ | $K_{d1}$ | μ |
| | | DMOA | 1.9509 | 1.9999 | 0.99766 | 0.50392 | 1.9993 | 1.0837 | 1.9985 | 0.72771 | 0.51402 |
| | | CFOA | 1.9635 | 1.9465 | 0.99283 | 0.52808 | 1.9918 | 1.08 | 1.9867 | 0.57825 | 0.72549 |
| Area Two | | | $K_1$ | $K_2$ | $K_3$ | $K_{p1}$ | $K_{i1}$ | λ | $K_{p2}$ | $K_{d1}$ | μ |
| | | DMOA | 1.5759 | 0.50608 | 0.86869 | 0.94871 | 1.5451 | 0.74817 | 1.9311 | 1.2956 | 0.72311 |
| | | CFOA | 1.2699 | 0.99446 | 0.92506 | 1.0926 | 1.4358 | 0.6723 | 1.11 | 0.59468 | 0.76925 |

To assess the efficacy of the proposed FLC, its performance is initially compared with fuzzy FOPID–PI controllers optimized by the CFOA and PSO algorithms [36]. A further comparison is performed with a fuzzy PID controller improved by the TLBO algorithm, alongside traditional PID controllers refined using LCOA, CFOA, and PSO techniques [37], all evaluated under uniform operating conditions. Table 5 presents the optimized gain values for these controllers.

**Table 5.** Optimized Gain Values of Different Controllers Using Various Algorithms [36].

| **Area** | **Controller** | **Algorithm** | **Parameters** | | | | | | | | |
|---|---|---|---|---|---|---|---|---|---|---|---|
| Area One | Fuzzy FOPID-PI | | $K_1$ | $K_2$ | $K_p$ | $K_i$ | $K_d$ | λ | μ | $K_{p1}$ | $K_{I1}$ |
| | | CFOA | 1.9998 | 1.9992 | 2 | 1.998 | 0.302 | 1 | 0.41315 | 2 | 1.0079 |
| | | PSO | 1.8901 | 2 | 1.6463 | 1.8904 | 0.5055 | 1 | 0.1598 | 1.5524 | 0.4903 |
| Area Two | | | $K_1$ | $K_2$ | $K_p$ | $K_i$ | $K_d$ | λ | μ | $K_{p1}$ | $K_{I1}$ |
| | | CFOA | 0.95497 | 1.8325 | 1.9165 | 1.9996 | 0.30887 | 0.0022093 | 0.99893 | 1.5102 | 0.10025 |
| | | PSO | 0.1011 | 2 | 1.6974 | 2 | 1.2743 | 0.3527 | 1 | 0.3622 | 1.1093 |
| | Fuzzy PID-TLBO | $K_1$ | $K_2$ | $K_3$ | $K_4$ | $K_5$ | $K_6$ | $K_7$ | $K_8$ | | |
| | | 1.9857 | 1.9968 | 1.687 | 1.9876 | 1.3469 | 1.5512 | 0.809 | 0.5043 | | |
| | PIDs | $K_{P1}$ | $K_{I1}$ | $K_{D1}$ | $K_{P2}$ | $K_{I2}$ | $K_{D2}$ | | | | |
| | PID-LCOA | 0.939 | 0.7998 | 0.5636 | 0.5208 | 0.4775 | 0.708 | | | | |
| | PID-CFOA | 1.8147 | 2 | 1.1331 | 0.090157 | 1.6888 | 1.9988 | | | | |
| | PID-PSO | 1.9987 | 1.4469 | 0.79221 | 1.5327 | 0.73122 | 1.2484 | | | | |

DMOA and CFOA were assessed under identical tuning conditions, including the same ITAE cost function, parameter bounds, population size, iteration limit, simulation model, and disturbance scenario. The additional controllers adopted from the literature were examined under the same operating conditions to provide closed-loop performance benchmarks.

All simulations were conducted in MATLAB/Simulink (2024a), utilizing specific .m scripts for the implementation of the DMOA and CFOA optimization methods. A two-area power system model, incorporating the comprehensive controller framework and disturbance conditions, was constructed in the Simulink environment to guarantee reproducibility and precise real-time depiction. The suggested PIDF + Fuzzy FOPI–FOPD controller ex-

hibits enhanced damping performance and swift transient response in frequency deviations and tie-line power fluctuations, as depicted in Figures 8–10.

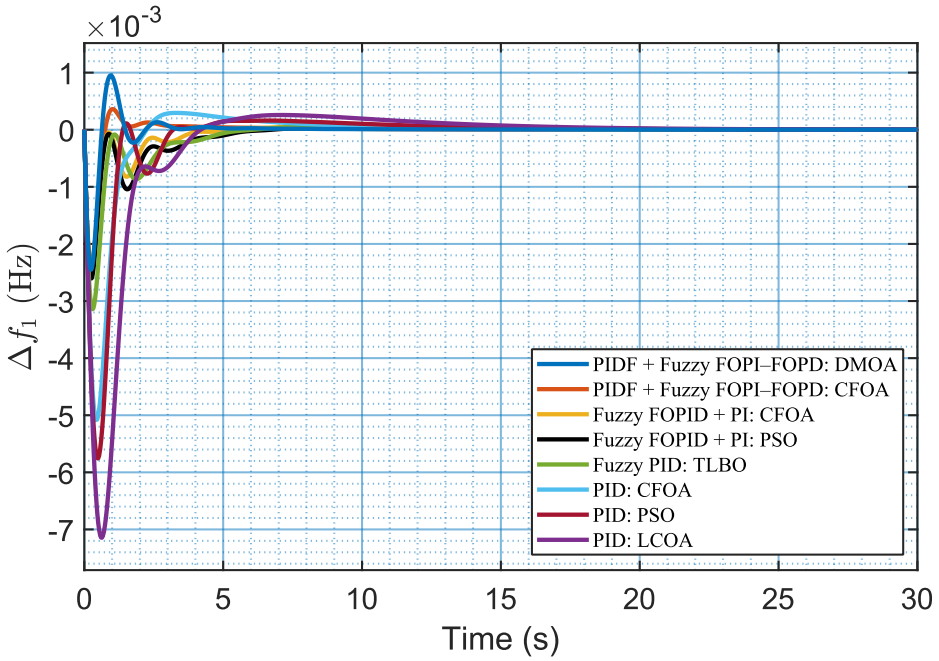


**Figure 8.** Frequency deviation in area 1.

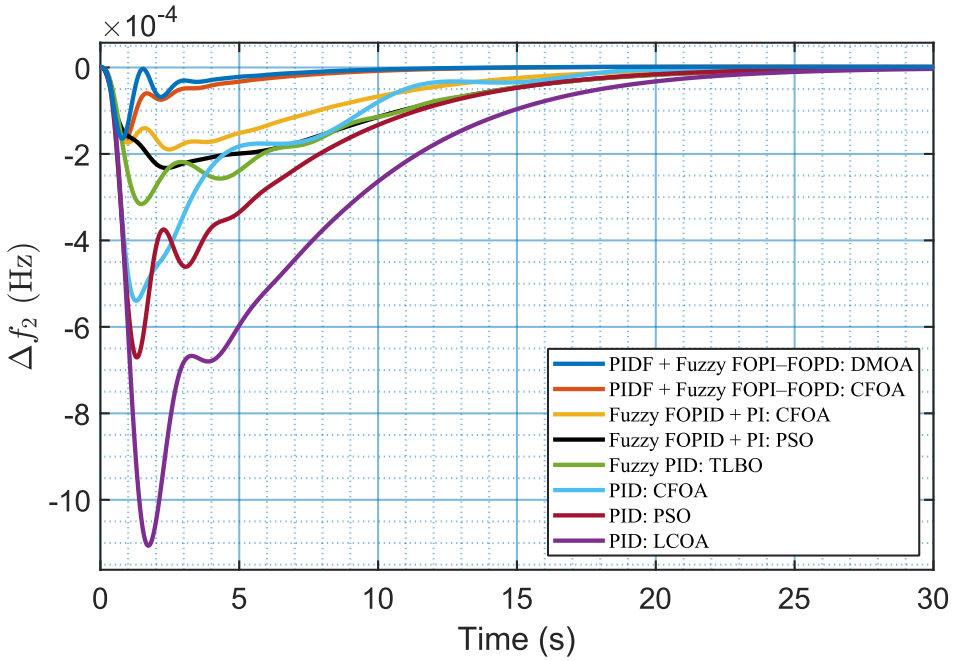


**Figure 9.** Frequency deviation in area 2.

The dynamic efficacy of the proposed PIDF + Fuzzy FOPI–FOPD controllers is evaluated by examining the frequency responses of both areas and the oscillatory behavior of tie-line power. Figure 8 demonstrates that the controller optimized by DMOA attains the minimal undershoot and the quickest settling response in Area 1, indicating robust damping performance under disturbance conditions. The CFOA-optimized controller demonstrates a robust and well-regulated response, significantly diminishing oscillations, but its undershoot and settling time are marginally greater than those of the DMOA-based configuration. Conversely, standard PID controllers, especially PID-LCOA, exhibit more

pronounced frequency dips and considerably extended settling times, underscoring their constrained robustness in dynamic operational contexts.

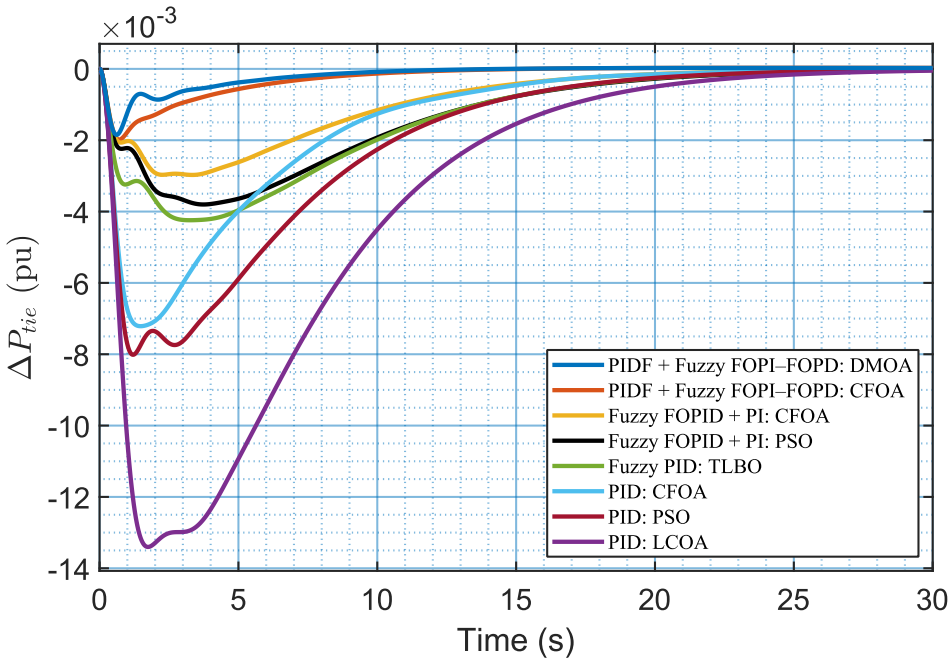


**Figure 10.** Tie-line power deviation.

A comparable trend is evident in Area 2 (Figure 9), where both fractional fuzzy controllers exhibit minimal overshoot and facilitate smooth convergence to the steady-state condition. Classical PID controllers exhibit somewhat slower transient recovery, with PID-LCOA displaying the most significant divergence and the least effective damping performance.

The tie-line power deviation data presented in Figure 10 further substantiates the efficacy of the suggested hybrid fuzzy-fractional strategy in mitigating inter-area power oscillations. The DMOA-optimized controller yields the minimal undershoot and the fastest stabilization, as indicated by the lowest ITAE value presented in Table 6. Although the CFOA-optimized controller operates consistently with well-damped and convergent responses, its ITAE value is moderately elevated compared to the DMOA model. In comparison, the PID-LCOA controller demonstrates the greatest tie-line deviation and the highest ITAE value, indicating its diminished efficacy in sustaining coordinated frequency management.

**Table 6.** Dynamic Response Metrics of Test System 1 for Different Controllers.

| Controller | F1 | | | F2 | | Tie Line Power | | ITAE |
|---|---|---|---|---|---|---|---|---|
| | OS | US | ST | US | ST | US | ST | |
| PIDF + Fuzzy-DMOA | $9.509 \times 10^{-4}$ | $-2.448 \times 10^{-3}$ | 3.1030 | $-1.646 \times 10^{-4}$ | 12.2404 | $-1.849 \times 10^{-3}$ | 13.5478 | 0.02939 |
| PIDF + Fuzzy-CFOA | $3.608 \times 10^{-4}$ | $-2.375 \times 10^{-3}$ | 4.3562 | $-1.704 \times 10^{-4}$ | 13.4575 | $-1.981 \times 10^{-3}$ | 14.4947 | 0.03937 |
| Fuzzy-CFOA | $4.8696 \times 10^{-5}$ | $-2.425 \times 10^{-3}$ | 3.9471 | $-1.897 \times 10^{-4}$ | 22.6711 | $-2.973 \times 10^{-3}$ | 23.0381 | 0.1992 |
| Fuzzy-PSO | $4.5279 \times 10^{-5}$ | $-2.601 \times 10^{-3}$ | 5.4909 | $-2.325 \times 10^{-4}$ | 24.3901 | $-3.802 \times 10^{-3}$ | 24.4230 | 0.3184 |
| Fuzzy-TLBO | $5.942 \times 10^{-5}$ | $-3.1422 \times 10^{-3}$ | 4.9936 | $-3.1594 \times 10^{-4}$ | 23.5188 | $-0.0042$ | 23.9377 | 0.3264 |
| PID-CFOA | $2.9454 \times 10^{-4}$ | $-5.087 \times 10^{-3}$ | 7.8827 | $-5.398 \times 10^{-4}$ | 17.9728 | $-7.214 \times 10^{-3}$ | 19.6328 | 0.2661 |
| PID-PSO | $1.6071 \times 10^{-4}$ | $-5.759 \times 10^{-3}$ | 9.3374 | $-6.707 \times 10^{-4}$ | 20.2334 | $-8.015 \times 10^{-5}$ | 21.3580 | 0.4094 |
| PID-LCOA | $2.578 \times 10^{-4}$ | $-7.147 \times 10^{-3}$ | 11.7031 | $-1.1064 \times 10^{-3}$ | 21.0698 | $-0.0134$ | 21.9780 | 0.7842 |

The findings indicate that the DMOA-tuned hybrid fuzzy controller provides the most balanced and resilient LFC performance, characterized by rapid transient recovery, robust

damping, and elevated steady-state accuracy. Simultaneously, the CFOA-tuned controller persists as a robust and efficient alternative, albeit with marginally inferior performance compared to DMOA, while traditional PID techniques persistently underperform across all assessed time-domain performance parameters.

### *4.2. Scenario 2: Power System 1 with GDB*

This subsection investigates the effect of Governor Dead Band (GDB) nonlinearities on the time-domain frequency-control response of the interconnected two-area system by activating the GDB block described in Equation (3) within the configuration illustrated in Figure 1. To isolate the impact of GDB on the obtained responses, the controller settings derived for the nominal linear case were applied directly, with no additional retuning. The responses under GDB operation are shown in Figures 11–13, and the associated performance metrics are summarized in Table 7.

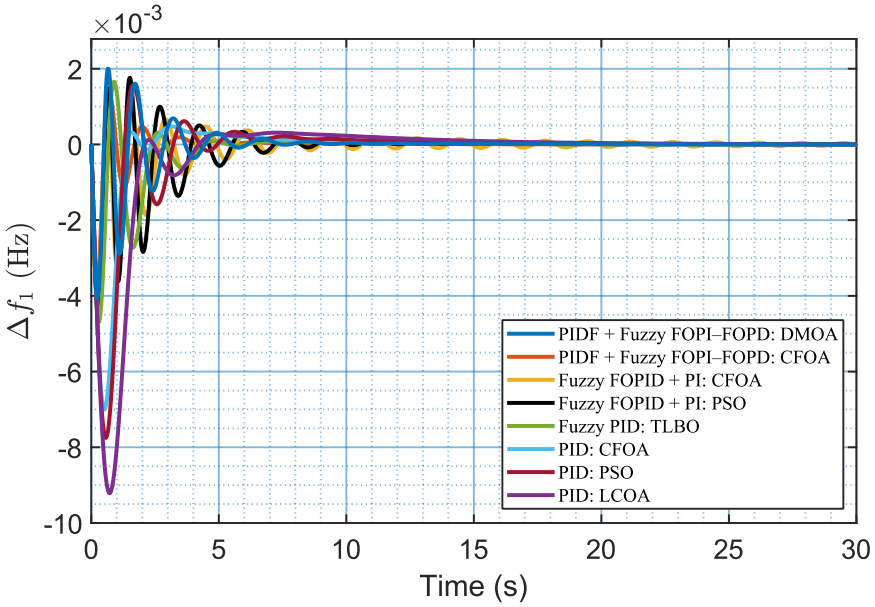


**Figure 11.** Frequency deviation in area 1.

The results indicate that the inclusion of GDB introduces pronounced nonlinear effects that significantly deteriorate transient performance, manifested through increased undershoot, prolonged settling times, and oscillatory behavior. In particular, the PIDF + Fuzzy FOPI–FOPD (DMOA) controller exhibits a clear degradation in performance. As reported in Table 7, the frequency response in Area 1 experiences an undershoot of $-4.060 \times 10^{-3}$ with a settling time of 7.0749 s, while Area 2 exhibits an undershoot of $-3.012 \times 10^{-4}$ and a settling time of 16.9532 s. Moreover, the tie-line power deviation records an undershoot of $-3.38 \times 10^{-3}$ with a settling time of 19.0416 s, resulting in an ITAE value of 0.1098, which reflects a noticeable loss of dynamic efficiency under GDB nonlinearity.

In contrast, the PIDF + Fuzzy FOPI–FOPD (CFOA) controller demonstrates a comparatively more bounded and recoverable dynamic response despite the presence of GDB. Specifically, Area 1 exhibits a reduced undershoot of $-3.707 \times 10^{-3}$ with a shorter settling time of 5.2020 s, while Area 2 stabilizes within 14.3778 s. The tie-line power deviation also settles faster at 16.3595 s, yielding a significantly lower ITAE value of 0.05845, which indicates improved damping capability and robustness against nonlinear disturbances.

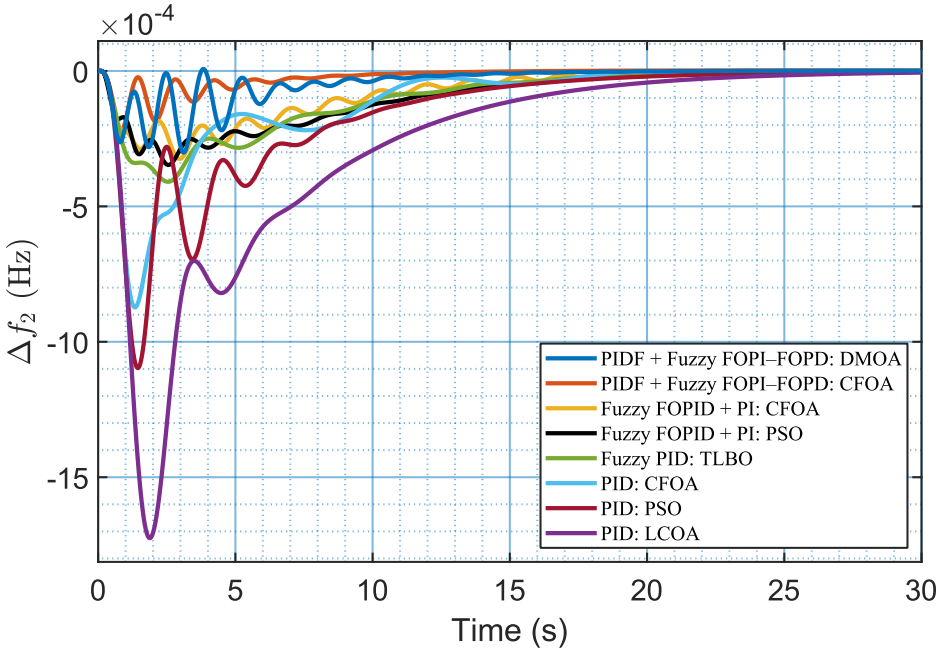


**Figure 12.** Frequency deviation in area 2.

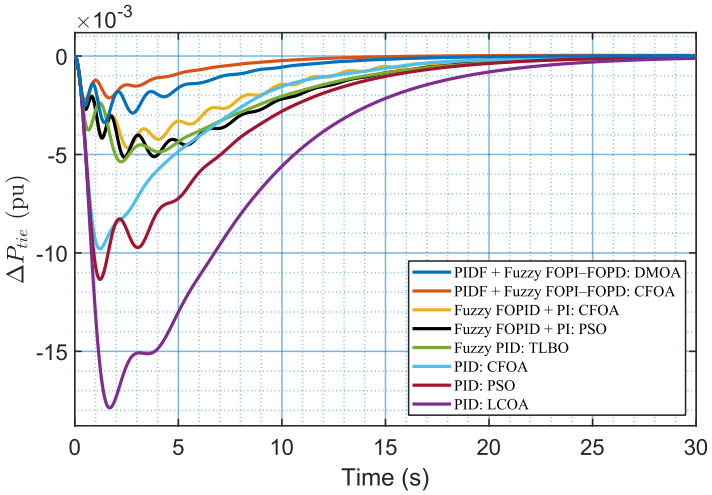


**Figure 13.** Tie-line power deviation.

**Table 7.** Test System 1 Metrics Under GDB for Different Controllers.

| Controller | F1 | | | F2 | | | Tie Line Power | | ITAE |
|---|---|---|---|---|---|---|---|---|---|
| | OS | US | ST | OS | US | ST | US | ST | |
| PIDF + Fuzzy-DMOA | $2.001 \times 10^{-3}$ | $-4.060 \times 10^{-3}$ | 7.0749 | $7.069 \times 10^{-6}$ | $-3.012 \times 10^{-4}$ | 16.9532 | $-3.38 \times 10^{-3}$ | 19.0416 | 0.1098 |
| PIDF + Fuzzy-CFOA | $1.352 \times 10^{-3}$ | $-3.707 \times 10^{-3}$ | 5.2020 | 0 | $-2.260 \times 10^{-4}$ | 14.3778 | $-2.26 \times 10^{-3}$ | 16.3595 | 0.05845 |
| Fuzzy-CFOA | $1.23 \times 10^{-3}$ | 0.0041 | 21.2599 | $1.60 \times 10^{-6}$ | $3.2488 \times 10^{-4}$ | 26.2991 | 0.0047 | 24.3810 | 0.3058 |
| Fuzzy-PSO | $1.758 \times 10^{-3}$ | 0.0042 | 13.0079 | 0 | $3.4702 \times 10^{-4}$ | 23.3911 | 0.0051 | 23.7700 | 0.383 |
| Fuzzy-TLBO | $1.65 \times 10^{-3}$ | 0.0047 | 4.9043 | 0 | $4.0913 \times 10^{-4}$ | 22.6947 | 0.0054 | 24.1230 | 0.3714 |
| PID-CFOA | $4.786 \times 10^{-4}$ | 0.0070 | 7.4226 | $6.43 \times 10^{-6}$ | $8.7313 \times 10^{-4}$ | 17.7911 | 0.0098 | 19.2478 | 0.3347 |
| PID-PSO | $1.576 \times 10^{-3}$ | 0.0078 | 8.2382 | 0 | 0.0011 | 19.0914 | 0.0113 | 21.5307 | 0.5258 |
| PID-LCOA | $3.110 \times 10^{-4}$ | 0.0092 | 11.1872 | 0 | 0.0017 | 20.3068 | 0.0179 | 22.7831 | 1.016 |

The standalone fuzzy controllers (Fuzzy-CFOA, Fuzzy-PSO, and Fuzzy-TLBO) provide limited damping performance, characterized by longer settling times exceeding 22 s in several cases and elevated ITAE values. Meanwhile, conventional PID controllers exhibit the weakest adaptability to GDB effects, with PID-LCOA producing the largest deviations and the highest ITAE value (1.016), underscoring its inadequacy under nonlinear operating conditions.

Overall, these findings reveal that although the DMOA-tuned controller delivers strong performance under linear conditions, its sensitivity to GDB nonlinearity leads to noticeable degradation in transient behavior. Conversely, the CFOA-tuned controller maintains better damping characteristics and more bounded transient responses under the same nonlinear constraints, highlighting the importance of incorporating nonlinear-aware optimization mechanisms in the LFC controller design.

The time-domain responses shown in Figures 8–13, together with the comparative results in Table 7, indicate that activating GDB nonlinearity markedly alters the overall response of the LFC system, resulting in greater undershoot magnitude, extended settling time, and oscillatory transients. An important observation is that the PIDF + Fuzzy FOPI–FOPD (DMOA) controller, although exhibiting enhanced performance under linear operating conditions, shows a marked deterioration in time-domain performance upon the introduction of GDB, leading to persistent oscillations and an inability to achieve steady-state convergence. Conversely, the PIDF + Fuzzy FOPI–FOPD (CFOA) controller, while previously marginally less effective than DMOA in the absence of GDB, exhibits convergent and recoverable dynamic behavior under GDB-affected situations, achieving constrained oscillations and a finite settling profile. This discrepancy underscores the necessity of assessing controller resilience not only under ideal settings but also amidst the practical nonlinear dynamics intrinsic to governor systems.

These observations highlight the imperative of incorporating GDB features in controller design to ensure reliable LFC performance in practical multi-area power systems, where nonlinearities are intrinsic rather than exceptional.

### *4.3. Scenario 3: Power System 2 Without Nonlinearities*

The proposed method was further validated for robustness and broader applicability by applying the controller to a different two-area power-system configuration shown in Figure 2, where a 0.05 pu step load perturbation was imposed in Area 1. In this case, the PIDF + Fuzzy FOPI–FOPD controller was employed, and its performance was assessed after tuning with the DMOA and CFOA. Following the same setup used previously, both optimizers were run for 100 iterations to determine the best controller settings, while the search interval for each gain was restricted to [0, 2]; the PIDF derivative filter coefficient $K_f$ was tuned over the broader range [0, 500]. The optimal gain values obtained from DMOA and CFOA are presented in Table 8, confirming the controller's suitability for different power-system configurations.

**Table 8.** Optimized Parameter Values of the PIDF + Fuzzy FOPI–FOPD Controller.

| Area | Controller | Algorithm | Parameters | | | | | | | | |
|---|---|---|---|---|---|---|---|---|---|---|---|
| Area One | PIDF | | $K_{p1}$ | | | $K_{i1}$ | | $K_{d1}$ | | $K_{f1}$ | |
| | | DMOA | 0.99573 | | | 1.9985 | | 0.50112 | | 100 | |
| | | CFOA | 0.66213 | | | 2 | | 0.5386 | | 441.58 | |
| Area Two | | | $K_{p2}$ | | | $K_{i2}$ | | $K_{d2}$ | | $K_{f2}$ | |
| | | DMOA | 1.9205 | | | 1.9625 | | 1.6956 | | 423.55 | |
| | | CFOA | 1.2788 | | | 0.82847 | | 1.8722 | | 191.08 | |
| **Area** | **Controller** | **Algorithm** | **Parameters** | | | | | | | | |
| Area One | Fuzzy FOPI–FOPD | | $K_1$ | $K_2$ | $K_3$ | $K_{p1}$ | $K_{i1}$ | $\lambda$ | $K_{p2}$ | $K_{d1}$ | $\mu$ |
| | | DMOA | 1.9999 | 1.7205 | 0.50037 | 0.51403 | 2 | 1.0364 | 1.9991 | 0.53428 | 0.90338 |
| | | CFOA | 1.9913 | 1.9992 | 0.74786 | 1.043 | 1.9894 | 0.9999 | 1.209 | 0.52507 | 0.76195 |
| Area Two | | | $K_1$ | $K_2$ | $K_3$ | $K_{p1}$ | $K_{i1}$ | $\lambda$ | $K_{p2}$ | $K_{d1}$ | $\mu$ |
| | | DMOA | 0.50013 | 1.7182 | 0.5816 | 1.9392 | 1.2808 | 0.64528 | 0.63637 | 1.9194 | 0.99105 |
| | | CFOA | 1.1375 | 1.3291 | 0.80024 | 1.9263 | 1.0254 | 0.59262 | 0.97047 | 1.3421 | 0.72326 |

Moreover, to assess the effectiveness of the proposed controller, its results were compared with other fuzzy-based control structures, including fuzzy FOPID–PI controllers tuned by CFOA and PSO [36], all examined under identical operating conditions. The corresponding optimized gain settings for these controllers are provided in Table 9, enabling a consistent comparison of performance across different controller structures and tuning approaches.

**Table 9.** Optimized Gain Values of Different Controllers Obtained with Various Algorithms [36].

| Area | Controller | Algorithm | Parameters | | | | | | | | |
|---|---|---|---|---|---|---|---|---|---|---|---|
| Area One | Fuzzy FOPID-PI | | $K_1$ | $K_2$ | $K_p$ | $K_i$ | $K_d$ | λ | μ | $K_{p1}$ | $K_{I1}$ |
| | | CFOA | 0.37564 | 0.84351 | 1.8576 | 0.45653 | 0.36982 | 0.38209 | 0.44983 | 0.88282 | 2 |
| | | PSO | 0.3163 | 0.4863 | 0.7276 | 1.1019 | 0.9564 | 0.0896 | 0.3475 | 0.7935 | 1.6199 |
| Area Two | | | $K_1$ | $K_2$ | $K_p$ | $K_i$ | $K_d$ | λ | μ | $K_{p1}$ | $K_{I1}$ |
| | | CFOA | 1.3611 | 1.3818 | 0.9252 | 1.4084 | 0.36194 | 0.64056 | 0.84815 | 1.8829 | 0.5525 |
| | | PSO | 0.5815 | 0.8611 | 0.5636 | 1.6106 | 1.2139 | 0.6321 | 0.0762 | 0.4790 | 1.4447 |

To strengthen the assessment of robustness and consistency, the proposed controllers were applied to a different interconnected two-area system layout, as illustrated in Figure 2, under their optimized linear settings. The responses presented in Figures 14–16, together with the gain values listed in Table 8 and the performance metrics summarized in Table 10, describe the system dynamics when a 0.05 pu step load perturbation is imposed on Area 1. The system responses unequivocally indicate that the PIDF + Fuzzy FO-PI–FOPD (DMOA) controller has the best transient performance, attaining the minimal undershoot and the swiftest settling time among all assessed signals. In Area 1, it attains an undershoot of $-3.587 \times 10^{-2}$ with a settling time of 0.8821 s, but the frequency in Area 2 and tie-line power deviations stabilize within 2.9970 s and 3.1833 s, respectively, yielding the minimal ITAE value of 0.02466.

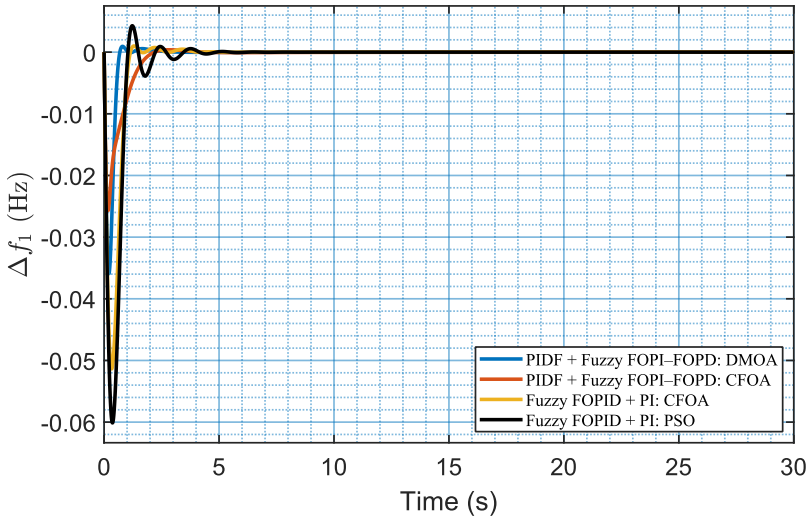


**Figure 14.** Frequency deviation in area 1.

The PIDF + Fuzzy FOPI–FOPD (CFOA) controller ensures well-damped and convergent responses, albeit with marginally extended settling times. It yields an undershoot of $-2.563 \times 10^{-2}$ in Area 1 with a settling time of 1.9419 s, whereas Area 2 and tie-line deviations converge in 3.7028 s and 3.8075 s, respectively, resulting in an ITAE of 0.06617.

Conversely, the independent fuzzy controllers demonstrate reduced convergence speed. The Fuzzy-CFOA configuration attains settling times of 1.0891 s in Area 1 and 3.6398 s in Area 2, while the Fuzzy-PSO controller exhibits the poorest performance,

characterized by the most significant undershoot ($-6.012 \times 10^{-2}$) and the longest settling times (2.1084 s in Area 1 and 4.0905 s in Area 2), in addition to the highest ITAE value of 0.09101.

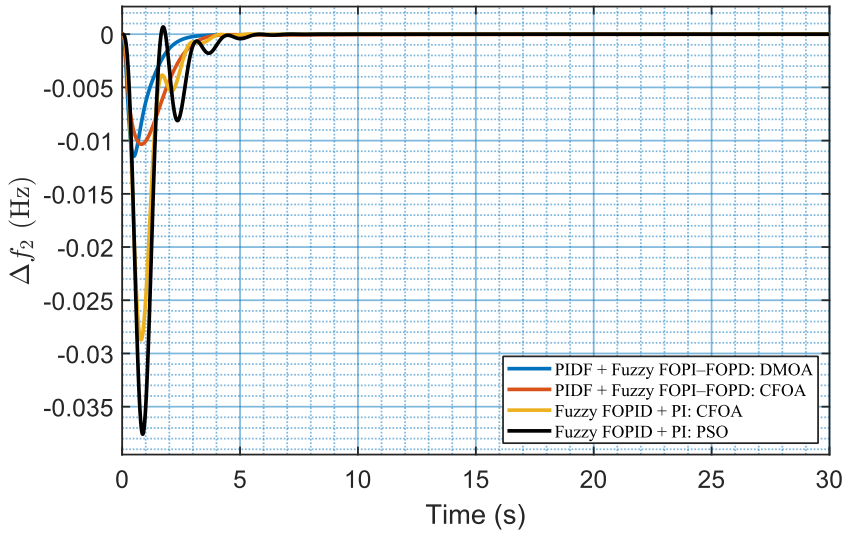


**Figure 15.** Frequency deviation in area 2.

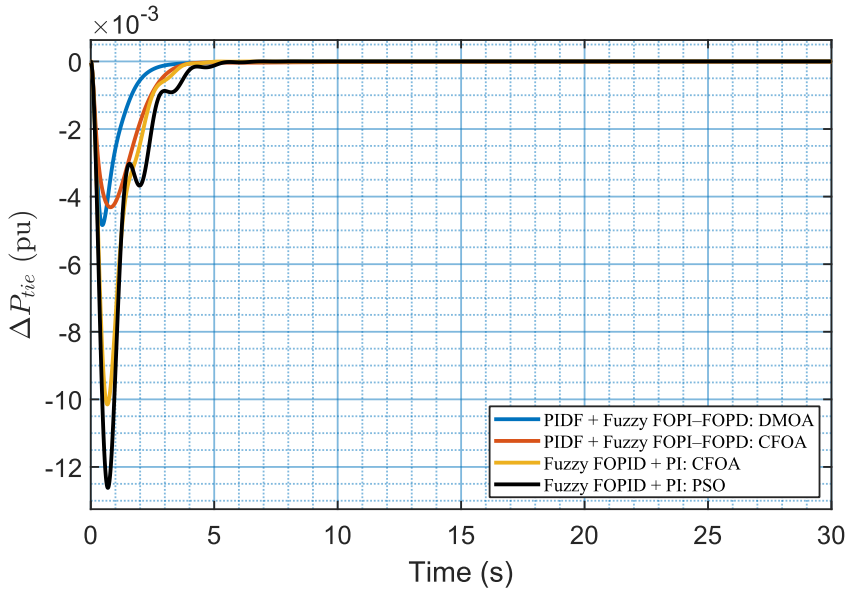


**Figure 16.** Tie-line power deviation.

**Table 10.** Dynamic Response Metrics of Test System 2 Using the Proposed Fuzzy LFC Scheme.

| Controller | F1 | | | F2 | | | Tie Line Power | | ITAE |
|---|---|---|---|---|---|---|---|---|---|
| | OS | US | ST | OS | US | ST | US | ST | |
| PIDF + Fuzzy-DMOA | $9.374 \times 10^{-4}$ | $-3.587 \times 10^{-2}$ | 0.8821 | 0 | $-1.148 \times 10^{-2}$ | 2.9970 | $-4.841 \times 10^{-3}$ | 3.1833 | 0.02466 |
| PIDF + Fuzzy-CFOA | $3.8314 \times 10^{-4}$ | $-2.563 \times 10^{-2}$ | 1.9419 | 0 | $-1.034 \times 10^{-2}$ | 3.7028 | $-4.315 \times 10^{-3}$ | 3.8075 | 0.06617 |
| Fuzzy-CFOA | $9.9816 \times 10^{-4}$ | $-5.131 \times 10^{-2}$ | 1.0891 | $7.1887 \times 10^{-6}$ | $-2.872 \times 10^{-2}$ | 3.6398 | $-1.015 \times 10^{-2}$ | 3.5664 | 0.06455 |
| Fuzzy-PSO | $4.275 \times 10^{-3}$ | $-6.012 \times 10^{-2}$ | 2.1084 | $6.802 \times 10^{-4}$ | $-3.758 \times 10^{-2}$ | 4.0905 | $-1.262 \times 10^{-2}$ | 3.9972 | 0.09101 |

These results indicate that DMOA offers the optimal tuning for System 2 under linear operating conditions, whereas CFOA serves as a robust alternative. Additionally, non-cascaded fuzzy controllers, especially those tuned with PSO, demonstrate inferior performance in achieving rapid and precise frequency regulation in LFC applications.

### *4.4. Scenario 4: Power System 2 with GRC*

This subsection investigates the effect of Generation Rate Constraints (GRC) on the time-domain frequency-control response of the interconnected two-area system by embedding the GRC block illustrated in Figure 3 within the configuration given in Figure 2. To isolate the dynamic contribution of GRC without introducing retuning-related bias, the fuzzy-controller parameters obtained for the nominal linear case were used unchanged. This procedure permits a direct assessment of the response variations attributable solely to GRC and draws attention to an issue that has received limited discussion in previous studies, especially the interaction between GRC dynamics and pre-tuned fuzzy control structures. The responses obtained with GRC are shown in Figures 17–19, while the controller gains adopted in this evaluation are listed in Tables 8 and 9.

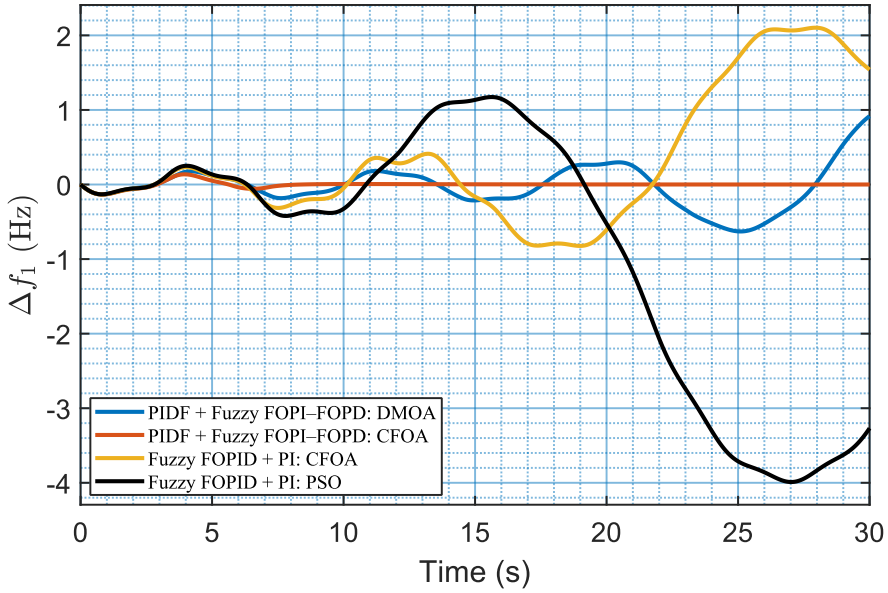


**Figure 17.** Frequency deviation in area 1.

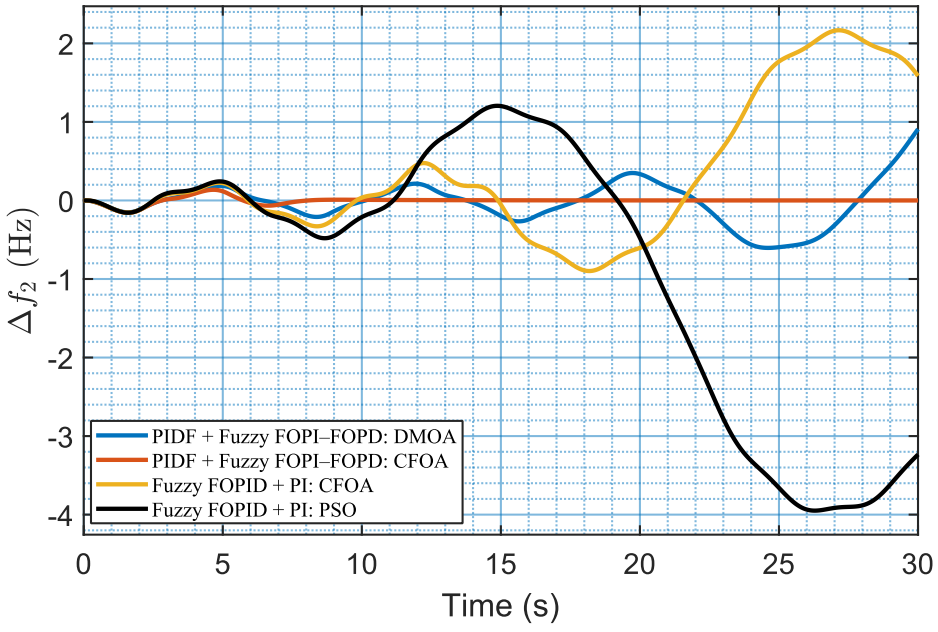


**Figure 18.** Frequency deviation in area 2.

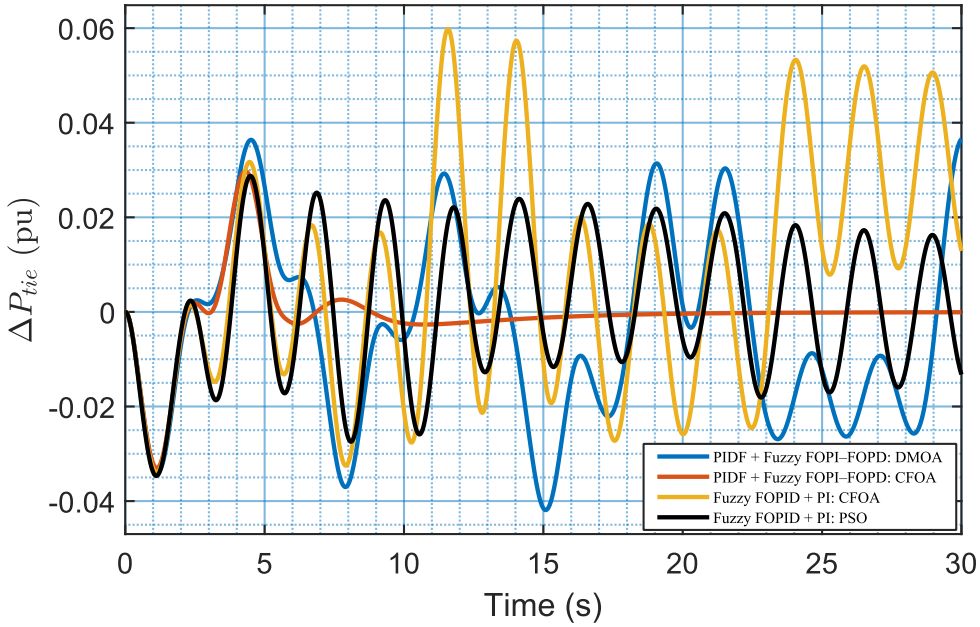


**Figure 19.** Tie-line power deviation.

The outcomes depicted in Figures 17–19 and encapsulated in Table 11 distinctly demonstrate the disparity in controller performance upon the introduction of GRC nonlinearity. Despite the PIDF + Fuzzy FOPI–FOPD (DMOA) controller demonstrating superior dynamic performance under optimal linear operating conditions, the introduction of GRC results in a significant deterioration of its performance. The DMOA-based controller demonstrates continuous oscillations in Area 1, Area 2, and tie-line power, failing to attain steady-state convergence (i.e., ST = N/A for all responses), and is associated with a notably elevated ITAE value of 255.2, signifying a total loss of acceptable frequency regulation performance. This study indicates that although DMOA operates efficiently in linear contexts, it demonstrates a deficiency in robustness when faced with real-world nonlinear operational constraints.

**Table 11.** Test System 2 Dynamic Response Metrics Under GRC for Different Controllers.

| Controller | F1 | | | F2 | | | TIE LINE | | | ITAE |
|---|---|---|---|---|---|---|---|---|---|---|
| | OS | US | ST | OS | US | ST | OS | US | ST | |
| PIDF + Fuzzy-DMOA | 0.2.976 | −0.6295 | N/A | 0.3494 | −0.6039 | N/A | 0.03637 | −0.04189 | N/A | 255.2 |
| PIDF + Fuzzy-CFOA | 0.1368 | −0.1341 | 15.0516 | 0.1358 | −0.1564 | 13.6945 | 0.0297 | −0.0330 | 17.1860 | 5.252 |
| Fuzzy-CFOA | 2.1027 | $-8.232 \times 10^{-1}$ | N/A | 2.1668 | $-8.984 \times 10^{-1}$ | N/A | $5.977 \times 10^{-2}$ | $-3.392 \times 10^{-2}$ | N/A | 878.3 |
| Fuzzy-PSO | 1.173 | −3.989 | N/A | 1.205 | −3.947 | N/A | $2.876 \times 10^{-2}$ | $-3.467 \times 10^{-2}$ | N/A | 1793 |

Conversely, the PIDF + Fuzzy FOPI–FOPD (CFOA) controller has a more bounded and convergent response under identical GRC conditions. The CFOA-based controller demonstrates regulated overshoot and undershoot, subsequently returning to steady-state gradually, with settling periods of 15.0516 s in Area 1, 13.6945 s in Area 2, and 17.1860 s for tie-line power, accompanied by a relatively lower ITAE value of 5.252. This illustrates an enhanced capacity to manage governor rate saturation and maintain bounded and convergent time-domain responses.

In contrast, the independent fuzzy controllers (Fuzzy-CFOA and Fuzzy-PSO) exhibit markedly inferior performance, evidenced by greater deviation magnitudes and a lack of significant settling behavior, resulting in substantially elevated ITAE values of 878.3 and 1793, respectively. This suggests that non-cascaded fuzzy structures are inadequate to counteract the nonlinear effects caused by GRC.

The results indicate that controller performance is significantly influenced by the operating environment. However, GRC nonlinearities significantly compromise the DMOA-based controller's performance, leading to non-convergent oscillatory behavior. Conversely, the CFOA-based controller exhibits a more steady and balanced response under the same conditions, progressively reinstating system equilibrium despite the existence of GRC. These discoveries underscore the necessity of integrating nonlinear constraints, such as GRC, into the tuning process to guarantee dependable and practically implementable LFC performance.

### *4.5. Scenario 5: Robustness Assessment Under Parametric Uncertainty*

Key plant parameters, namely the damping coefficient, speed regulation constant, system inertia, and the turbine and governor time constants vary continuously because of operating fluctuations, environmental influences, and equipment aging. Such variations can noticeably affect closed-loop control behavior; however, their role in LFC applications has not been investigated in sufficient depth. In general, higher system inertia tends to delay the transient response, while a larger damping coefficient usually improves frequency recovery. Conversely, increases in the turbine or governor time constants often aggravate frequency deviations.

This subsection evaluates the performance of the proposed PIDF + Fuzzy FOPI–FOPD controller, optimized by CFOA, under significant parametric uncertainty in a two-area interconnected power system with GDB nonlinearity. For this purpose, eight independent test scenarios are defined in Table 12 by varying key system parameters—namely the inertia constant (H), damping coefficient (D), regulation constant (R), turbine time constant (Tt), governor time constant (Tg), and frequency bias factor (B)—by ±35% from their nominal values. The optimal gain values of the proposed PIDF + Fuzzy FOPI–FOPD (CFOA) controller, listed in Table 4, are kept unchanged for all test scenarios, and no re-optimization is performed. In this way, any observed performance variation can be attributed solely to parameter changes rather than controller retuning.

**Table 12.** Examined Cases of System Parametric Uncertainty [36].

| Case Number | Uncertain Parameter | Base Value (Area 1) | Base Value (Area 2) | Applied Change | Updated Value (Area 1) | Updated Value (Area 2) |
|---|---|---|---|---|---|---|
| Case 1 | H | 5 | 4 | +35% | 6.75 | 5.4 |
| Case 2 | D | 0.6 | 0.9 | −35% | 0.39 | 0.585 |
| Case 3 | R | 0.05 | 0.0625 | +35% | 0.0675 | 0.0844 |
| Case 4 | Tt | 0.5 | 0.6 | −35% | 0.325 | 0.39 |
| Case 5 | B | 20.6 | 16.9 | +35% | 27.81 | 22.815 |
| Case 6 | D | 0.6 | 0.9 | +35% | 0.81 | 1.215 |
| Case 7 | Tg | 0.2 | 0.3 | −35% | 0.13 | 0.195 |
| Case 8 | R | 0.05 | 0.0625 | −35% | 0.0325 | 0.0406 |

Figures 20–22 present the frequency responses of Areas 1 and 2, along with the tie-line power variances, over the eight parametric uncertainty scenarios. The graphical results demonstrate that the PIDF + Fuzzy FOPI–FOPD (CFOA) controller sustains steady and limited performance despite significant fluctuations (±35%) in critical system parameters. Table 13 summarizes the relevant quantitative performance indices, including overshoot (OS), undershoot (US), settling time (ST), and ITAE values for all situations.

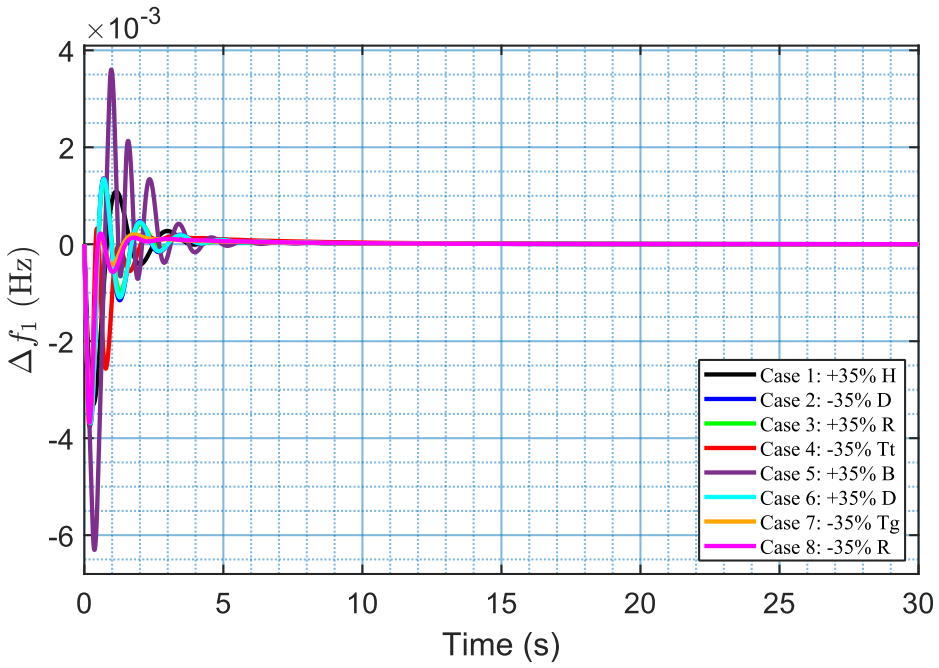


**Figure 20.** Frequency deviation in area 1.

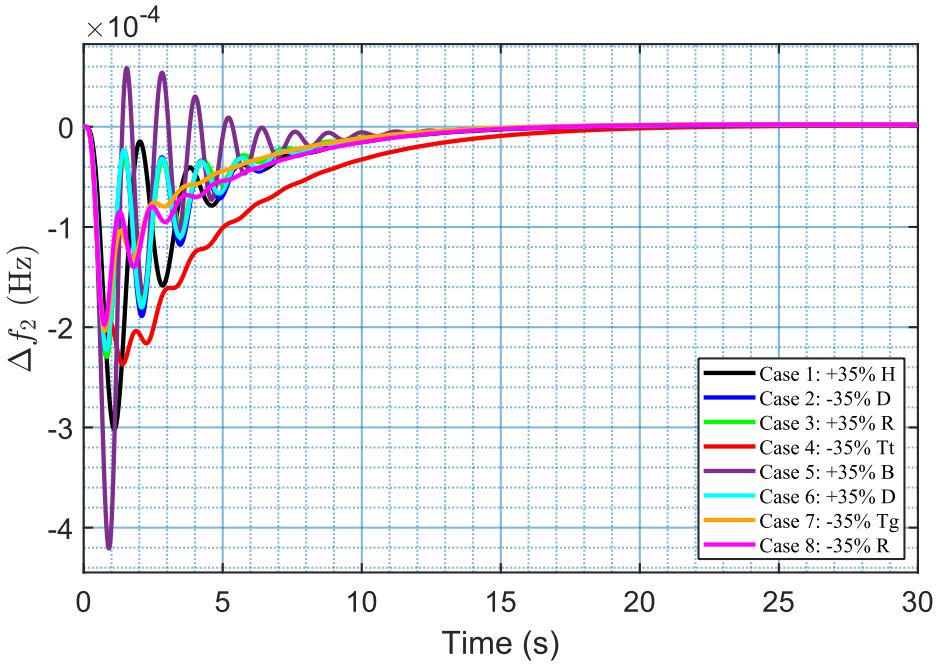


**Figure 21.** Frequency deviation in area 2.

The results demonstrate that the proposed controller maintains robust performance under all operating conditions. In Case 1 (+35% in inertia constant H), the controller successfully restricts overshoot in Area 1 to $1.086 \times 10^{-3}$ and undershoot to $-3.31 \times 10^{-3}$, achieving a settling time of 5.3632 s, while the tie-line stabilizes at 15.9240 s, thereby confirming the retention of damping capability despite the augmented system inertia. Cases 2 and 6, linked to alterations in the damping coefficient (D), exhibit the most rapid settling behavior, with Area 1 settling periods of 5.2117 s and 5.1900 s, respectively, signifying enhanced oscillation suppression under elevated damping circumstances.

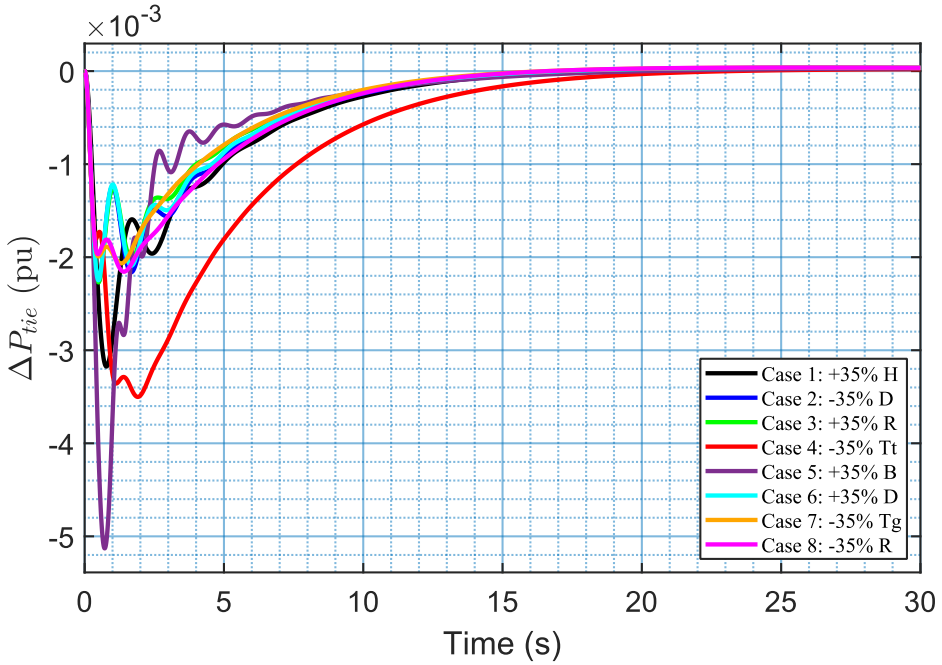


**Figure 22.** Tie-line power deviation.

**Table 13.** System Dynamic Response Under Different Parametric Uncertainty Cases Using the Fuzzy Controller.

| Case Number | F1 | | | F2 | | | Tie Line | | ITAE |
|---|---|---|---|---|---|---|---|---|---|
| | OS | US | ST | OS | US | ST | US | ST | |
| Case 1 | $1.086 \times 10^{-3}$ | $-3.31 \times 10^{-3}$ | 5.3632 | 0 | $-3.19 \times 10^{-4}$ | 13.9646 | $-3.174 \times 10^{-3}$ | 15.9240 | 0.06393 |
| Case 2 | $1.357 \times 10^{-3}$ | $-3.719 \times 10^{-3}$ | 5.2117 | 0 | $-2.29 \times 10^{-4}$ | 14.4751 | $-2.267 \times 10^{-3}$ | 16.5827 | 0.05985 |
| Case 3 | $1.291 \times 10^{-3}$ | $-3.703 \times 10^{-3}$ | 5.0573 | 0 | $-2.294 \times 10^{-4}$ | 13.8848 | $-2.27 \times 10^{-3}$ | 16.1387 | 0.05438 |
| Case 4 | $3.225 \times 10^{-4}$ | $-3.752 \times 10^{-3}$ | 6.1932 | 0 | $-2.37 \times 10^{-4}$ | 18.1124 | $-3.501 \times 10^{-3}$ | 18.8389 | 0.144 |
| Case 5 | $3.601 \times 10^{-3}$ | $-6.305 \times 10^{-3}$ | 4.6625 | $5.848 \times 10^{-5}$ | $-4.207 \times 10^{-4}$ | 10.8670 | $-5.129 \times 10^{-3}$ | 14.3478 | 0.05339 |
| Case 6 | $1.344 \times 10^{-3}$ | $-3.690 \times 10^{-3}$ | 5.1900 | 0 | $-2.228 \times 10^{-4}$ | 14.3758 | $-2.248 \times 10^{-3}$ | 16.3029 | 0.05772 |
| Case 7 | $2.021 \times 10^{-4}$ | $-3.657 \times 10^{-3}$ | 3.6966 | 0 | $-2.036 \times 10^{-4}$ | 14.2719 | $-2.066 \times 10^{-3}$ | 16.1059 | 0.05383 |
| Case 8 | $2.206 \times 10^{-4}$ | $-3.668 \times 10^{-3}$ | 4.4984 | 0 | $-1.974 \times 10^{-4}$ | 15.3009 | $-2.156 \times 10^{-3}$ | 16.0906 | 0.06086 |

By contrast, Case 4, characterized by a $-35\%$ variance in turbine time constant (Tt), yields the highest ITAE value of 0.144, indicating a heightened demand for control effort yet, the response remains free of sustained oscillations, and all deviations converge to steady state. In all remaining scenarios, both overshoot and undershoot are consistently minimal (e.g., Area 1 US ranging from $-3.66 \times 10^{-3}$ to $-3.31 \times 10^{-3}$), while tie-line settling periods range from 14.27 to 18.88 s, thereby affirming dependable inter-area coordination.

In summary, the PIDF + Fuzzy FOPI–FOPD (CFOA) controller exhibits significant resilience and consistent dynamic performance amidst various parametric uncertainties without necessitating gain retuning. This robustness highlights the controller's practical applicability in real-world LFC situations, where system parameters fluctuate regularly and re-optimization is frequently impractical during operation.

### *4.6. Scenario 6: Impact of Random Load Disturbance*

To examine the robustness of the proposed PIDF + Fuzzy FOPI–FOPD controller in Power System 1 (Figure 1) under GDB conditions, a three-step random load disturbance was applied only to Area 1. As illustrated in Figure 23, the disturbance begins at 0.01 p.u., rises to 0.025 p.u. at 5 s, and then drops to 0.005 p.u. at 15 s, thereby representing abrupt and asymmetrical load variations over a 30-s operating period.

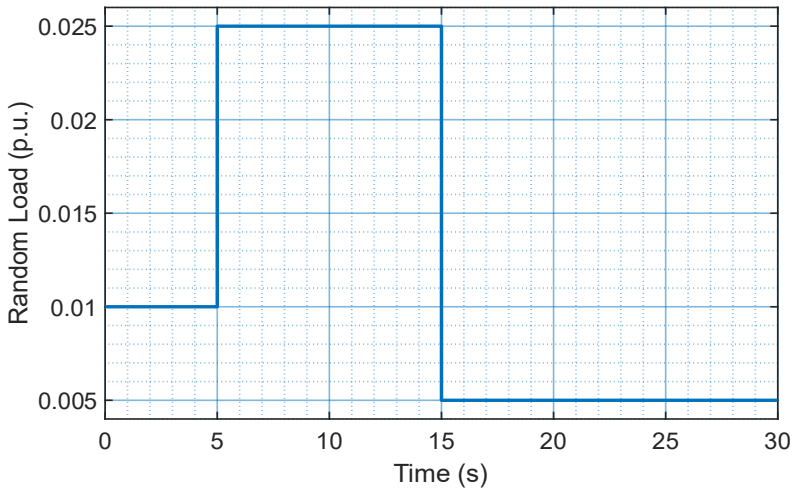


**Figure 23.** Random load disturbance profile.

Under this non-periodic and unpredictable disturbance pattern, the proposed hybrid PIDF + Fuzzy FOPI–FOPD controller, tuned by DMOA and CFOA, exhibited favorable adaptability and strong disturbance-handling capability. Its performance was compared with Fuzzy FOPID + PI-CFOA, Fuzzy FOPID + PI-PSO, Fuzzy PID-TLBO, and conventional PID-CFOA, PID-PSO, and PID-LCOA, all evaluated under the same system conditions. For the frequency and tie-line deviation signals (Δf1, Δf2, and ΔPtie), the proposed scheme produced the lowest OS/US values and the shortest ST. Its capacity to accommodate sudden load increases and decreases without sustained oscillatory behavior further indicates effective performance under variable disturbance conditions. The corresponding dynamic responses in Area 1, Area 2, and the tie-line are presented in Figures 24–26, respectively, showing the improved transient behavior of the proposed controller.

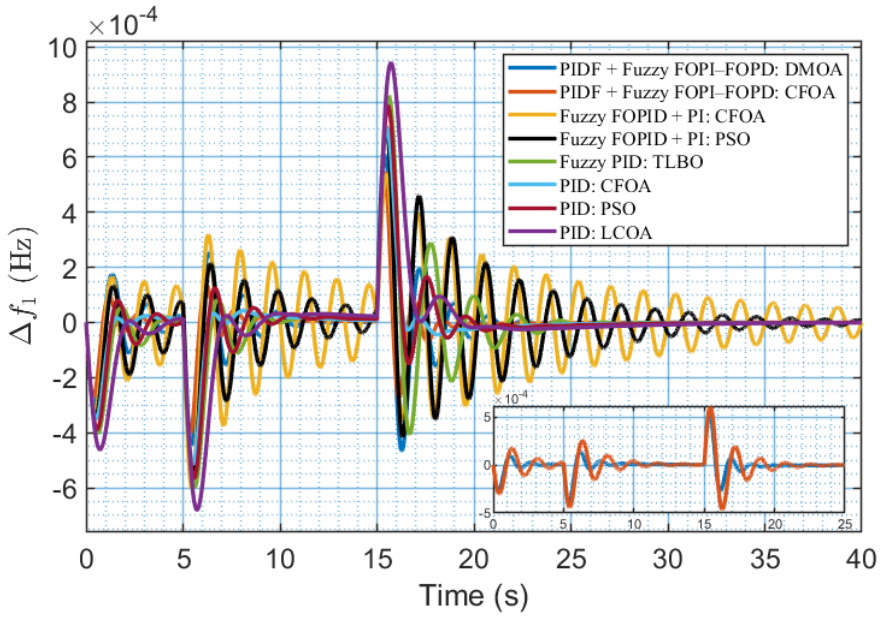


**Figure 24.** Dynamic Response Under Random Load Disturbance in Area 1.

This test scenario reflects practical operating conditions, including renewable-energy integration and industrial load switching, and therefore supports the practical relevance of the proposed controller for LFC applications.

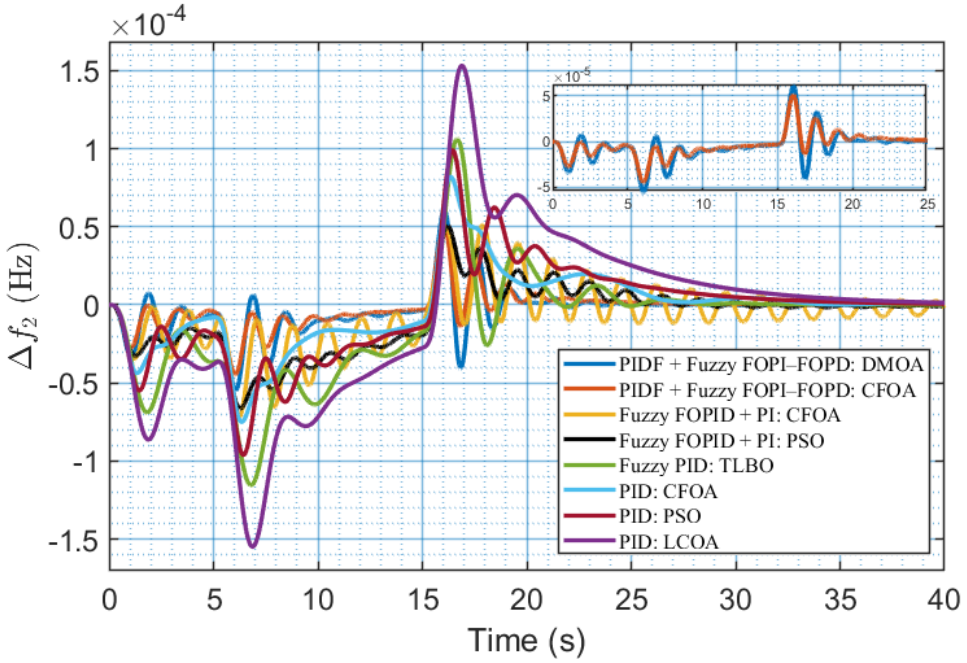


**Figure 25.** Dynamic Response Under Random Load Disturbance in Area 2.

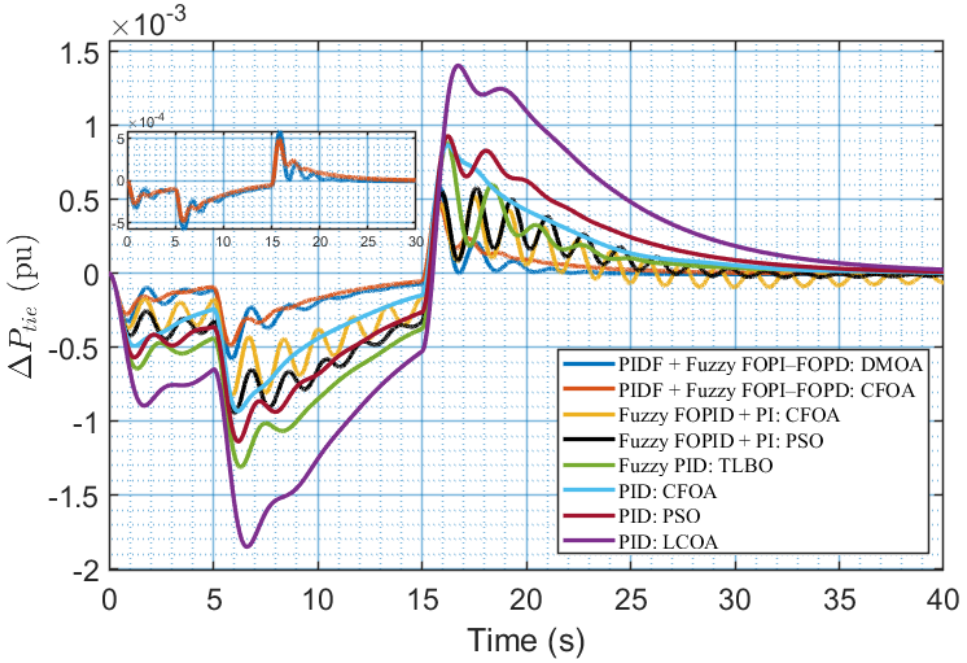


**Figure 26.** Dynamic Response Under Random Load Disturbance in the Tie-Line.

The proposed PIDF + Fuzzy FOPI–FOPD control scheme demonstrates strong capability in mitigating random load disturbances, while maintaining bounded and convergent dynamic responses under varying operating conditions. By contrast, the benchmark controllers, namely Fuzzy FOPID + PI-CFOA, Fuzzy FOPID + PI-PSO, Fuzzy PID-TLBO, and the conventional PID-CFOA, PID-PSO, and PID-LCOA, show weaker performance under time-varying demand patterns, indicating lower adaptability to rapidly changing loads. The obtained results show that the hybrid controller can accommodate sudden and stochastic load variations while preserving acceptable dynamic performance. These findings further support its suitability for practical implementation in modern LFC applications under realistic load uncertainty.

## 5. Conclusions and Future Work

The present study introduced a sophisticated LFC method utilizing a hybrid PIDF + Fuzzy FOPI–FOPD controller, optimized through two advanced metaheuristic algorithms: the Dwarf Mongoose Optimization Algorithm (DMOA) and the Catch Fish Optimization Algorithm (CFOA). The suggested hybrid architecture adeptly integrates the predictive features of fractional-order dynamics, the adaptive reasoning of fuzzy logic, and the structured damping characteristics of classical proportional-integral-derivative control to attain enhanced frequency regulation in multi-area interconnected power systems.

Extensive simulations were performed on two benchmark systems under both linear and nonlinear operating conditions, incorporating the impacts of Governor Dead Band (GDB) and Generation Rate Constraint (GRC) nonlinearities. The results indicated that under optimal linear conditions, the PIDF + Fuzzy FOPI–FOPD (DMOA) controller attained superior transient performance, yielding the minimal undershoot and the quickest settling time across all frequency and tie-line responses. Nevertheless, the introduction of nonlinearities, such as GRC, caused the DMOA-based system to exhibit considerable oscillations and non-convergent oscillatory behavior, preventing it from achieving steady-state convergence. Conversely, the PIDF + Fuzzy FOPI–FOPD (CFOA) controller maintained bounded and convergent responses and ensured smooth convergence, exhibiting mild transient degradation while sustaining equilibrium in all test scenarios.

The CFOA-based controller demonstrated significantly enhanced performance in nonlinear settings, exhibiting diminished overshoot and undershoot magnitudes, as well as considerably lower ITAE values in comparison to both the fuzzy-only and traditional PID methods. These findings confirm the resilience and adaptability of CFOA in controlling complex nonlinearities, whereas DMOA, despite its efficacy in linear systems, demonstrated diminished robustness.

The work emphasizes the necessity of integrating nonlinear constraints, such as GDB and GRC, during the controller optimization phase to guarantee realistic and dependable performance in contemporary power grids. The suggested PIDF + Fuzzy FOPI–FOPD (CFOA) controller constitutes a practically feasible solution with well-damped and convergent responses for next-generation LFC applications, effective in limiting frequency deviations and preserving inter-area coordination even amidst significant nonlinear disturbances.

This study's positive results suggest several intriguing avenues for future research:

1. Experimental Implementation and Hardware Verification: Executing the proposed hybrid PIDF + Fuzzy FOPI–FOPD controller on embedded platforms, such as DSP or FPGA-based real-time systems, to empirically validate its performance and resilience against real-world disruptions.
2. Integration with Renewable-Dominant Hybrid Microgrids: Expanding the controller's functionality to intricate hybrid networks that incorporate renewable energy sources, including wind, photovoltaic (PV), and hydro units, alongside energy storage systems, to assess frequency regulation performance and response convergence under fluctuating resource availability.
3. Adaptive and Self-Learning Optimization Strategies: Improving the existing optimization framework by integrating adaptive or hybrid learning mechanisms—such as reinforcement learning or deep neuroevolutionary to facilitate online adjustment of controller parameters in response to fluctuating operating conditions.
4. Scalability and Multi-Area Coordination: Examining the scalability of the proposed control methodology in extensive interconnected power systems comprising many regions, with an emphasis on synchronized frequency regulation and tie-line power management among various controllers.

5. Enhanced Nonlinear and Uncertainty Modeling: Incorporating supplementary nonlinear effects such as turbine backlash, governor saturation, and load-side dynamics, alongside uncertainty modeling of renewable sources and communication networks, to thoroughly evaluate controller resilience in contemporary smart grid environments.

**Author Contributions:** Conceptualization, S.A., F.A., M.P., M.A. and M.S.; Methodology, S.A., F.A., M.P., M.A. and M.S.; Software, S.A., F.A., M.P., M.A. and M.S.; Validation, S.A., F.A., M.P., M.A. and M.S.; Formal analysis, S.A., F.A., M.P., M.A. and M.S.; Investigation, S.A., F.A., M.P., M.A. and M.S.; Resources, S.A., F.A., M.P., M.A. and M.S.; Data curation, S.A., F.A., M.P., M.A. and M.S.; Writing—original draft, S.A., F.A., M.P., M.A. and M.S.; Writing—review & editing, S.A., F.A., M.P., M.A. and M.S.; Visualization, S.A., F.A., M.P., M.A. and M.S.; Supervision, S.A., F.A., M.P., M.A. and M.S.; Project administration, S.A., F.A., M.P., M.A. and M.S.; Funding acquisition, S.A., F.A. and M.P. All authors have read and agreed to the published version of the manuscript.

**Funding:** This research received no external funding.

**Data Availability Statement:** The original contributions presented in this study are included in the article. Further inquiries can be directed to the corresponding author.

**Acknowledgments:** The authors would like to thank Cardiff University for paying the APC towards publishing this manuscript.

**Conflicts of Interest:** The authors declare no conflicts of interest.

## Abbreviations

The following abbreviations are used in this manuscript:

| | |
|---|---|
| LFC | Load frequency control |
| FOPID | Fractional order proportional-integral-derivative |
| PI | Proportional and integral |
| FLC | Fuzzy logic controller |
| CFOA | Catch fish optimization algorithm |
| ITAE | Integral of time-weighted absolute error |
| GDB | Governor dead band |
| GRC | Generation rate constraint |
| DMOA | Dwarf Mongoose Optimization algorithm |
| PSO | Particle swarm optimization |
| GA | Genetic algorithm |
| ITEA | Integral of time multiplied error in area |
| ACE | Area control error |
| MF | Membership function |
| NB | Negative big |
| NS | Negative small |
| Z | Zero |
| PS | Positive small |
| PB | Positive big |
| SLP | Step load perturbation |
| DG | Distributed generation |
| BES | Battery energy storage |
| SMES | Superconducting magnetic energy storage |
| RES | Renewable energy sources |
| AVR | Automatic voltage regulator |
| TLBO | Teaching–learning-based optimization |
| PIDF | Proportional, integral, derivative with filter |
| FOPI | Fractional order proportional-integral |
| FOPD | Fractional order proportional-derivative |

## Appendix A

The nominal parameters adopted for the two-area power system model are:

F = 60 Hz; $R_1$ =0.05 MW/Hz; $R_2$ =0.0625 MW/Hz; $B_1$ =20.6 Hz/MW; $B_2$ =16.9 Hz/MW; SLP = 0.2 pu; $T_{g1}$ =0.2 s; $T_{g2}$ =0.3 s; $T_{t1}$ =0.5 s; $T_{t2}$ =0.6 s; $H_1$ =5; $H_2$ =4; $D_1$ =0.6; $D_2$ =0.9; T = 2.

## Appendix B

The nominal parameters adopted for the two-area power system model are:

F = 60 Hz; $R_1 = R_2$ =0.05 MW/Hz; $B_1 = B_2$ =0.425 Hz/MW; SLP = 0.05 pu; $T_{g1} = T_{g2}$ =0.08 s; $T_{t1} = T_{t2}$ =0.3 s; $T_{P1} = T_{P2}$ =20 s; $K_{P1} = K_{P2}$ =120; $a_{12}$ =−1; $T_{12}$ =0.545.

## References


1. Gulzar, M.M.; Sibtain, D.; Alqahtani, M.; Alismail, F.; Khalid, M. Load frequency control progress: A comprehensive review on recent development and challenges of modern power systems. *Energy Strat. Rev.* **2025**, *57*, 101604. [CrossRef]
2. Hu, B.; Cai, J.; Xing, Z.; Zhang, P.; Wang, D.; Folly, K.A. Control and optimization techniques for load frequency control of multi-area Cyber–Physical Power Systems: A literature review. *Annu. Rev. Control.* **2025**, *60*, 101009. [CrossRef]
3. Khan, I.A.; Mokhlis, H.; Mansor, N.N.; Illias, H.A.; Awalin, L.J.; Wang, L. New trends and future directions in load frequency control and flexible power system: A comprehensive review. *Alex. Eng. J.* **2023**, *71*, 263–308. [CrossRef]
4. Shankar, R.; Pradhan, S.; Chatterjee, K.; Mandal, R. A comprehensive state of the art literature survey on LFC mechanism for power system. *Renew. Sustain. Energy Rev.* **2017**, *76*, 1185–1207. [CrossRef]
5. Shouran, M.; Anayi, F.; Packianather, M. A State-of-the-Art Review on LFC Strategies in Conventional and Modern Power Systems. In Proceedings of the 2021 International Conference on Advance Computing and Innovative Technologies in Engineering (ICACITE), Greater Noida, India, 4–5 March 2021; pp. 268–277. [CrossRef]
6. AboRas, K.M.; Sedik, A.M.; Hammad, M.R. Hybrid dual-area power grid frequency fluctuation effective control utilizing a maiden combination of MOA-based 1 + PIID and PDμFλ controllers. *Sci. Prog.* **2025**, *108*, 00368504251330521. [CrossRef]
7. Kozák, Š. State-of-the-art in control engineering. *J. Electr. Syst. Inf. Technol.* **2014**, *1*, 1–9. [CrossRef]
8. Ekinci, S.; Izci, D.; Turkeri, C.; Smerat, A.; Ezugwu, A.E.; Abualigah, L. Frequency regulation of two-area thermal and photovoltaic power system via flood algorithm. *Results Control. Optim.* **2025**, *18*, 100539. [CrossRef]
9. Abd-Elazim, S.M.; Ali, E.S. Load frequency controller design of a two-area system composing of PV grid and thermal generator via firefly algorithm. *Neural Comput. Appl.* **2016**, *30*, 607–616. [CrossRef]
10. Tuan, D.H.; Thanh, V.N.N.; Chi, D.N.; Pham, V.H. Improving Frequency Control of Multi-Area Interconnected Hydro-Thermal Power System Using PSO Algorithm. *Appl. Sci.* **2025**, *15*, 2898. [CrossRef]
11. Sharma, A.; Singh, N. Load frequency control of connected multi-area multi-source power systems using energy storage and lyrebird optimization algorithm tuned PID controller. *J. Energy Storage* **2024**, *100*, 113609. [CrossRef]
12. Almutairi, S.Z.; Moustafa, G.; Hakmi, S.H.; Shaheen, A.M. Bonobo Optimizer Inspired PI-(1+DD) Controller for Robust Load Frequency Management in Renewable Wind Energy Systems. *Int. J. Energy Res.* **2025**, *2025*, 6874402. [CrossRef]
13. Gopi, P.; Alluraiah, N.C.; Kumar, P.H.; Bajaj, M.; Blazek, V.; Prokop, L. Improving load frequency controller tuning with rat swarm optimization and porpoising feature detection for enhanced power system stability. *Sci. Rep.* **2024**, *14*, 1–15. [CrossRef] [PubMed]
14. Mohamed, M.A.E.; Jagatheesan, K.; Anand, B. Modern PID/FOPID controllers for frequency regulation of interconnected power system by considering different cost functions. *Sci. Rep.* **2023**, *13*, 1–29. [CrossRef] [PubMed]
15. El-Rifaie, A.M.; Abid, S.; Ginidi, A.R.; Shaheen, A.M. Fractional Order PID Controller Based-Neural Network Algorithm for LFC in Multi-Area Power Systems. *Eng. Rep.* **2025**, *7*, 70028. [CrossRef]
16. Gupta, D.K.; Dei, G.; Soni, A.K.; Jha, A.V.; Appasani, B.; Bizon, N.; Srinivasulu, A.; Nsengiyumva, P. Fractional order PID controller for load frequency control in a deregulated hybrid power system using Aquila Optimization. *Results Eng.* **2024**, *23*, 102442. [CrossRef]
17. Shawqran, A.M.; Attia, M.A.; Mekhamer, S.F.; Kotb, H.; Ibrahim, M.A.; Mordi, A. Enhancing Load Frequency Control in Power Systems Using Hybrid PIDA Controllers Optimized with TLBO-TS and TLBO-EDO Techniques. *Processes* **2025**, *13*, 1532. [CrossRef]
18. Izci, D.; Ekinci, S.; Çelik, E.; Bajaj, M.; Blazek, V.; Prokop, L. Dynamic load frequency control in Power systems using a hybrid simulated annealing based Quadratic Interpolation Optimizer. *Sci. Rep.* **2024**, *14*, 1–19. [CrossRef]
19. Bhupathiraju, S.R.; Pedakota, K.R. Load Frequency Control of Hybrid Power System with PIDD Controller in Presence of Electric Vehicles. 2024. Available online: https://journal.esrgroups.org/jes/article/view/6261 (accessed on 5 February 2025).

20. Biswas, D.K.; Debbarma, S.; Singh, P.P. LFC of multi-area power system using a robust full-order terminal sliding mode controller considering communication delay. *Electr. Eng.* **2025**, *107*, 4421–4435. [CrossRef]
21. Van Huynh, V.; Naqvi, S.; Nguyen, B.L.-H.; Tran, A.-T.; Shim, J.W.; Do, T.D. Robust super-twisting algorithm-based single-phase sliding mode frequency controller in power systems integrating wind turbines and energy storage systems. *Sci. Rep.* **2025**, *15*, 19740. [CrossRef]
22. Roy, T.K.; Saha, S.; Oo, A.M.T. An Optimised Adaptive Integral Sliding Mode Control Approach for Multi-Area Power Systems: Enhancing LFC Robustness and Stability with RES Integration and Time-Delay Mitigation. *IET Energy Syst. Integr.* **2025**, *7*, e70006. [CrossRef]
23. Gautam, V.V.; Loka, R.; Parimi, A.M. Cubature Kalman filter and linear quadratic regulator for load frequency control. *Electr. Power Syst. Res.* **2023**, *222*, 109509. [CrossRef]
24. Garg, R.; Mittal, A.; Syed, K.; Asim, M.; Chakravorty, A.; Goyal, S. Linear Quadratic Regulator (LQR)-Based Load Frequency Control in Power Systems. In Proceedings of the 2024 2nd World Conference on Communication & Computing (WCONF), Raipur, India, 12–14 July 2024; pp. 1–6. [CrossRef]
25. Amiri, F.; Hatami, A. Load frequency control for two-area hybrid microgrids using model predictive control optimized by grey wolf-pattern search algorithm. *Soft Comput.* **2023**, *27*, 18227–18243. [CrossRef]
26. Mokhtar, M.; Marei, M.I.; Sameh, M.A.; Attia, M.A. An Adaptive Load Frequency Control for Power Systems with Renewable Energy Sources. *Energies* **2022**, *15*, 573. [CrossRef]
27. Rahangdale, C.K.; Shukla, S.P.; Singh, S.K. Automatic Generation Control Using Model Reference Adaptive Control (MRAC) Scheme in a Multi Area Power System. *NeuroQuantology* **2021**, *19*, 811–820. Available online: https://neuroquantology.com/open-access/Automatic+Generation+Control+Using+Model+Reference+Adaptive+Control+%2528MRAC%2529+Scheme+in+a+Multi+Area+Power+System_12490/ (accessed on 5 February 2025).
28. Nohra, C.; Ghandour, R.; Khaled, M.; Outbib, R. A Novel H∞/$H_2$ Pole Placement LFC Controller with Measured Disturbance Feedforward Action for Disturbed Interconnected Power Systems. *Automation* **2025**, *6*, 90. [CrossRef]
29. Limon, F.A.; Upoma, R.S.; Sinha, N.; Swarna, S.R.; Nath, B.K.; Khanum, K.; Rahman, J.; Iqbal, S. Grey wolf optimization-based fuzzy-PID controller for load frequency control in multi-area power systems. *J. Autom. Intell.* **2025**, *4*, 145–159. [CrossRef]
30. Ranjan, M.; Shankar, R. Effect of Electric Vehicles and Renewable Sources on Frequency Regulation in Hybrid Power System Using QOAOA Optimized Type-2 Fuzzy Fractional Controller. *Int. J. Fuzzy Syst.* **2024**, *26*, 825–848. [CrossRef]
31. Feleke, S.; Pydi, B.; Satish, R.; Kotb, H.; Alenezi, M.; Shouran, M. Frequency Stability Enhancement Using Differential-Evolution- and Genetic-Algorithm-Optimized Intelligent Controllers in Multiple Virtual Synchronous Machine Systems. *Sustainability* **2023**, *15*, 13892. [CrossRef]
32. Shouran, M.; Anayi, F.; Packianather, M.; Habil, M. Different Fuzzy Control Configurations Tuned by the Bees Algorithm for LFC of Two-Area Power System. *Energies* **2022**, *15*, 657. [CrossRef]
33. Mouassa, S.; Alateeq, A.; Alassaf, A.; Bayindir, R.; Alsaleh, I.; Jurado, F. Optimal Power Flow Analysis with Renewable Energy Resource Uncertainty Using Dwarf Mongoose Optimizer: Case of ADRAR Isolated Electrical Network. *IEEE Access* **2024**, *12*, 10202–10218. [CrossRef]
34. Moustafa, G.; Smaili, I.H.; Almalawi, D.R.; Ginidi, A.R.; Shaheen, A.M.; Elshahed, M.; Mansour, H.S.E. Dwarf Mongoose Optimizer for Optimal Modeling of Solar PV Systems and Parameter Extraction. *Electronics* **2023**, *12*, 4990. [CrossRef]
35. Alnefaie, S.A.; Alkuhayli, A.; Al-Shaalan, A.M. Optimizing Load Frequency Control of Multi-Area Power Renewable and Thermal Systems Using Advanced Proportional–Integral–Derivative Controllers and Catch Fish Algorithm. *Fractal Fract.* **2025**, *9*, 355. [CrossRef]
36. Almutairi, S.; Anayi, F.; Packianather, M.; Shouran, M. An Innovative LFC System Using a Fuzzy FOPID-Enhanced via PI Controller Tuned by the Catch Fish Optimization Algorithm Under Nonlinear Conditions. *Sustainability* **2025**, *17*, 5966. [CrossRef]
37. Sahu, B.K.; Pati, S.; Mohanty, P.K.; Panda, S. Teaching–learning based optimization algorithm based fuzzy-PID controller for automatic generation control of multi-area power system. *Appl. Soft Comput.* **2015**, *27*, 240–249. [CrossRef]
38. Barakat, M. Novel chaos game optimization tuned-fractional-order PID fractional-order PI controller for load–frequency control of interconnected power systems. *Prot. Control. Mod. Power Syst.* **2022**, *7*, 1–20. [CrossRef]
39. Ali, E.; Abd-Elazim, S. BFOA based design of PID controller for two area Load Frequency Control with nonlinearities. *Int. J. Electr. Power Energy Syst.* **2013**, *51*, 224–231. [CrossRef]
40. Sahu, R.K.; Panda, S.; Padhan, S. A hybrid firefly algorithm and pattern search technique for automatic generation control of multi area power systems. *Int. J. Electr. Power Energy Syst.* **2015**, *64*, 9–23. [CrossRef]

41. Almutairi, S.; Anayi, F.; Packianather, M.; Shouran, M. An Optimal Two-Stage Tuned PIDF + Fuzzy Controller for Enhanced LFC in Hybrid Power Systems. *Sustainability* **2025**, *17*, 9109. [CrossRef]
42. Agushaka, J.O.; Ezugwu, A.E.; Abualigah, L. Dwarf Mongoose Optimization Algorithm. *Comput. Methods Appl. Mech. Eng.* **2022**, *391*, 114570. [CrossRef]